Global Climate Impacts of Greenland and Antarctic Meltwater: A Comparative Study

Qian Li[a] , John Marshall[a] , Craig D. Rye[a,b] , Anastasia Romanou[b] , David Rind[b] , and Maxwell Kelley[b]

[a] *Department of Earth, Atmospheric, and Planetary Sciences, Massachusetts Institute of Technology, Cambridge, MA, USA*

[b] *NASA Goddard Institute for Space Studies, New York, NY, USA*

Corresponding author: Qian Li, qian_li@mit.edu

ABSTRACT: Both the Greenland and Antarctic ice sheets have been melting at an accelerating rate over recent decades. Meltwater from Greenland might be expected to initiate a climate response which is distinct, and perhaps different from, that associated with Antarctic meltwater. Which one might elicit a greater climate response, and what mechanisms are involved? To explore these questions, we apply "Climate Response Functions (CRFs)" to guide a series of meltwater perturbation experiments using a fully-coupled climate model. In both hemispheres, meltwater drives atmospheric cooling, sea-ice expansion, and strengthened Hadley and Ferrel cells. Greenland meltwater induces a slowdown of the Atlantic Meridional Overturning Circulation (AMOC) and a cooling of the subsurface ocean in the northern high-latitudes. Antarctic meltwater, instead, induces a slowdown of the Antarctic Bottom Water formation and a warming of the subsurface ocean around Antarctica. For melt-rates up to 2000 Gt yr^{-1}, the climate response is rather linear. However, as melt-rates increase to 5000 Gt yr^{-1}, the climate response becomes non-linear. Due to a collapsed AMOC, the climate response is *super-linear* at high Greenland melt-rates. Instead, the climate response is *sub-linear* at high Antarctic melt-rates, due to the halting of the northward expansion of Antarctic sea ice by warm surface waters. Finally, in the linear limit, we use CRFs and linear convolution theory to make projections of important climate parameters in response to meltwater scenarios, which suggest that Antarctic meltwater will become a major driver of climate change, dominating that of Greenland meltwater, as the current century proceeds.

SIGNIFICANCE STATEMENT: Melting of the Greenland and Antarctic ice sheets is one of the most uncertain potential contributors to future climate change. In this study, we address the comparative role of Greenland and Antarctic meltwater in the climate system and explore the differing mechanisms at work in each hemisphere. We find that the climate response is linear for low melt-rates but becomes non-linear for high melt-rates. As the century proceeds, we speculate that Antarctic meltwater will increasingly dominate that of Greenland meltwater, leading to atmospheric cooling, Antarctic sea-ice expansion, and contraction and warming of the Antarctic Bottom Water. Greenland meltwater will instead affect smaller changes local to the North Atlantic.

1. Introduction

The Greenland and Antarctic ice sheets represent the largest land store of freshwater over the globe which, should they completely melt and flow into the ocean, could contribute a total of 7.5 m and 58 m to global mean sea level, respectively (Morlighem et al. 2017; Fretwell et al. 2013). Recent observations have shown that these ice sheets are melting at an accelerating rate (Paolo et al. 2015; Rignot et al. 2019; Mouginot et al. 2019; Shepherd et al. 2018, 2020; King et al. 2020). Between 1992–2011 and 2012–2017, the rate of ice mass loss has risen from roughly 100 Gt yr^{-1} to 250 Gt yr^{-1} in Greenland (Shepherd et al. 2020) and from 75 Gt yr^{-1} to roughly 200 Gt yr^{-1} in Antarctica (Shepherd et al. 2018). Since the 1990s, their combined contribution to global mean sea level has been 18 mm, of which 10 mm came from Greenland (Shepherd et al. 2020) and 8 mm from Antarctica (Shepherd et al. 2018). The Greenland ice mass loss is ice-sheet-wide owing to rapidly increasing surface melting and ice dynamical imbalances (King et al. 2020). The Antarctic ice sheet retreat is largely due to ice-shelf basal melt and iceberg calving in roughly equal magnitude along the periphery, primarily in the Amundsen-Bellingshausen Sea sectors (West Antarctica), Wilkes Land (East Antarctica), and the West and Northeast Peninsula (Rignot et al. 2019). Twenty-first-century simulations of the Greenland and Antarctic ice sheets forced with time-evolving ocean and climate fields derived from a high-emission scenario, suggest the projected melt-rates exceeding 500 Gt yr^{-1} and 5000 Gt yr^{-1} by 2100, respectively, leading to a total sea level rise in excess of 250 mm with meltwater feedback (Golledge et al. 2019).

Meltwater from Greenland and Antarctica contributes not only to sea level but also initiates climate change through its effect, for example, on sea-ice extent and the ocean's overturning

circulation. One might expect the impacts of Greenland meltwater to be different from that of Antarctic meltwater, because they act in different hemispheres and perturb different parts of the climate system. For example, it is thought that Antarctic meltwater spreading to the proximal ocean initiates surface cooling and freshening trends across the Southern Ocean (Bronselaer et al. 2018; Rye et al. 2020). Enhanced basal melt of Antarctic ice shelves (Rignot et al. 2013; Depoorter et al. 2013; Adusumilli et al. 2020) can cause significant sea-ice expansion by suppressing convective mixing and its associated vertical heat exchange (Hellmer 2004; Bintanja et al. 2013). Meltwater discharge along the Antarctic continental shelf tends to weaken the Antarctic Bottom Water (AABW) formation and abyssal ocean overturning (Silvano et al. 2018; Lago and England 2019; Li et al. 2023). Meltwater discharge from Greenland, meanwhile, can reduce deep ocean ventilation via a slowdown in the formation rate of North Atlantic Deep Water (NADW) originating in the Nordic (Greenland-Iceland-Norwegian (GIN)) Seas (Böning et al. 2016), and a slowdown of the Atlantic Meridional Overturning Circulation (AMOC) (Rahmstorf et al. 2015; Bakker et al. 2016). Antarctic meltwater can also affect the AMOC, but the sense of the change remains controversial. Stouffer et al. (2007) found that the AMOC remains unchanged or slightly weakened due to Antarctic meltwater spreading across the sea surface in the North Atlantic. However, Weaver et al. (2003) suggested that Antarctic meltwater rather intensifies the strength of the AMOC and NADW formation via a change in the potential density relationship between water masses. But then, these effects are damped by Greenland meltwater. Such competing climate impacts become even more intriguing when it is realized that increasing differences between Greenland and Antarctic melt-rates are expected, with the Antarctic source likely to increasingly dominate over Greenland in the coming decades (Golledge et al. 2019).

Addressing these issues is important, not least to explore the uncertainties in climate projections undertaken for the latest Coupled Model Intercomparison Project Phase 6 (CMIP6; Eyring et al. 2016). These projections do not account for dynamic ice sheet melt, thus lacking a key component of the cryosphere system. That said, many recent climate model simulations have applied meltwater scenarios either around Greenland (Hu et al. 2011; Bakker et al. 2016; Putrasahan et al. 2019; Orihuela-Pinto et al. 2022) or Antarctica (Bakker and Prange 2018; Bronselaer et al. 2018; Rye et al. 2020; Mackie et al. 2020; Beadling et al. 2022). Taken together, these studies suggest that Greenland meltwater is projected to weaken the AMOC significantly by 2100 in both intermediate

and high emission scenarios (Hu et al. 2011; Bakker et al. 2016), although intermodel differences are still evident (Bakker et al. 2016). By 2100 under a high-emission scenario, Antarctic meltwater is projected to drive a series of notable changes, inducing a decrease in global-mean surface air temperature, an increase in Antarctic sea-ice extent, a northward shift of Intertropical Convergence Zone, and Antarctic coastal warming associated with a marked on-shelf intrusion of warm Circumpolar Deep Water (Bronselaer et al. 2018).

The primary motivation of the current study is (i) to identify the key mechanisms which control the response of the climate system to Greenland and Antarctic meltwater, and (ii) to quantify the efficacy of Greenland vs. Antarctic meltwater in instigating global climate change. We will contrast the impacts of Greenland and Antarctic meltwater through a series of perturbation experiments using a fully-coupled climate model. We undertake three sets of experiments in which the same amount of meltwater is released along the land-ocean boundary of Greenland and Antarctica, both separately and together. We carry out the experiments in the framework provided by "Climate Response Functions (CRFs)" and linear convolution theory (Hasselmann et al. 1993). Here, the CRFs represent the response of climate parameters to a step-change in meltwater forcing, and the response to a linear-ramp forcing can be inferred by convolution to the extent that the response is linear. As successfully applied in many previous studies (Gregory et al. 2015; Marshall et al. 2014, 2017a; Rye et al. 2020; Lembo et al. 2020), this framework enables us to compare the relative contributions of different hemispheric meltwater sources on the global climate.

Our paper is organized as follows. In Section 2, the coupled model and experimental design are described. Sections 3 and 4 respectively contrast the global impacts and mechanisms in response to Greenland and Antarctic meltwater. Section 5 discusses the response functions for meltwater forcing and their application to make future projections of climatically important parameters, such as surface air temperature, sea-ice extent and strength of the AMOC. Finally, in Section 6, we discuss and conclude.

2. The coupled model and experimental design

a. The global climate model

We employ the E2.1-G version of the National Aeronautics and Space Administration (NASA) Goddard Institute for Space Studies (GISS) Earth system model, denoted GISS-E2.1-G (Kelley et al.

2020; Miller et al. 2021; Nazarenko et al. 2022). GISS-E2.1-G is a coupled climate model designed to simulate the earth system comprising representations of the atmosphere, ocean, land and sea ice. The atmospheric model component has a horizontal resolution of 2°× 2.5° latitude by longitude and 40 vertical pressure layers. The vertical coordinate transitions from a terrain-following sigma tropospheric representation below 150 hPa to constant-pressure stratospheric layers above this level, all the way up to the model top at 0.1 hPa. In this E2.1-G version, a new option facilitates a smooth transition centered at 100 hPa with a half-width of approximately 30 hPa. The dynamical core, atmospheric mixing, convection and boundary layer models are described in more detail in (Kelley et al. 2020).

The ocean model component of E2.1-G version has a horizontal resolution of 1°× 1.25° latitude by longitude and 40 vertical layers. It is mass-conserving with a free surface and natural surface boundary conditions for heat and freshwater fluxes (Russell et al. 1995). The model employs a version of the boundary layer K-profile parameterization (KPP) of vertical mixing (Large et al. 1994) and the Gent and McWilliams (GM) parameterization (Gent et al. 1995) with variable coefficients (Visbeck et al. 1997) for eddy tracer fluxes induced by mesoscale baroclinic turbulence. In E2.1-G, the parameterization of mesoscale eddy transport is updated with a moderate-complexity 3-D mesoscale diffusivity inspired by the studies presented in Marshall et al. (2017b). The vertical diapycnal diffusivity incorporates a new tidal mixing scheme via a dissipation distribution given by Jayne (2009), which improves the representation of the AMOC. Additional developments include the use of higher-order advection schemes (Prather 1986), finer upper-ocean layering and more realistic representation of flow through straits that affect property distributions in marginal seas (Kelley et al. 2020).

The sea-ice model component consists of two mass layers within each of which are two thermal layers. Sea ice salinity and tracer values are calculated on the atmospheric grid in the horizontal and the mass layers in the vertical. Sea-ice dynamics is based on a formulation of the standard viscous-plastic rheology (Zhang and Rothrock 2000). Sea-ice thermodynamics includes a "Brine Pocket" parameterization (Bitz and Lipscomb 1999) that allows salt to play a more active role in the specific heat and melt-rates of the sea ice.

The ice sheet model has no representation of ice flow dynamics, and its iceberg calving rates are determined (Tournadre et al. 2016), for each ice sheet, as those balancing its accumulation

of mass from precipitation minus evaporation and surface melt (Schmidt et al. 2014). Iceberg calving fluxes into the adjacent oceans are adjusted over 10 years time-lagged relative to the ice sheet accumulation, which is operative to represent ice sheet dynamics timescales in the model background state.

The GISS-E2.1-G model has a substantially improved climatology in a long pre-industrial control simulation, particularly in its representation of the Southern Hemisphere atmosphere, ocean and sea-ice distributions — see Kelley et al. (2020) and Miller et al. (2021). Our model simulates a notably realistic mixed layer depth distribution in the Southern Ocean (Supplementary Figs. S1a and S1c), suggesting that convection forms in plausible locations along the Antarctic continental shelf. However, the modeled mixed layers are too deep in the North Atlantic (Supplementary Figs. S1b and S1d), suggesting that there is excessive mixing with deep ocean waters (Lerner et al. 2021). The modeled seasonal cycle of Antarctic sea ice also agrees rather well with observations (Kelley et al. 2020). The wintertime Arctic sea-ice extent, however, exceeds that seen in observations, perhaps due to excess heat loss to the atmosphere (Kelley et al. 2020).

b. Experimental design

Here we consider three scenarios in which meltwater is released along the land-ocean boundary of Greenland or Antarctica, both separately and together, as summarised in Table 1. Then, a step-function forcing is applied in which the melt-rate is instantaneously stepped up from zero to 500 Gt yr^{-1} (~0.016 Sv) in one experiment, 2000 Gt yr^{-1} (~0.06 Sv) in another and finally 5000 Gt yr^{-1} (~0.16 Sv) to yield three experiments for each scenario, or nine in all (Figs. 1a-c). These amplitudes are inspired by the current and projected melt-rates ranging from several hundred up to 5000 Gt yr^{-1} by 2100, as noted in the Introduction. We follow the algorithm and procedure described in Rye et al. (2020). The meltwater fluxes and associated cooling anomalies, stemming from extraction of the latent heat required to melt ice, are distributed over the upper 200 meters, making use of the mask of the iceberg array as shown in Fig. 2. Note that we impose the meltwater perturbation in the near-surface layers, neglecting spatial complexity due to the contribution of basal melt at depth. In addition, we distribute the meltwater perturbation evenly along the continental margins, in an attempt to represent the lateral dispersion of freshwater from the coast. The model's background ocean circulation advects the implied sea surface salinity (SSS) anomalies away from

the coast along freshwater pathways, as an approximate alternative to the advection of icebergs away from the margin.

In order to contrast the global impacts and mechanisms of meltwater alone over the next several decades, all nine idealized meltwater perturbation experiments are initiated from a long pre-industrial control of 5,650 years and then run on in parallel for 50 years. The experiments in which a relatively small perturbation of 500 Gt yr^{-1} is carried out employ ten ensemble members. This, through averaging, enables us to dampen the effect of internal variability. Experiments, which assume much larger perturbations of 2000 Gt yr^{-1} and 5000 Gt yr^{-1}, have a more robust response and so need only employ one ensemble member. For the analyses of CRFs and convolutions, all the simulations are extended out to 150 years. This enables us to explore longer timescales and particularly temporal variability of the AMOC. The control experiments with pre-industrial forcings carried out alongside these perturbations do not employ any meltwater forcing. The difference between concurrent periods of perturbation and control is analyzed to minimize the influence of model drift on our results.

Note that in our figures the range of the colormap scales linearly with the magnitude of three meltwater forcings, enabling us to examine the linearity of atmospheric and ocean responses to meltwater forcing.

c. Freshwater pathways

We first check the behavior of our solutions by examining the temporal evolution and spatial distribution of SSS anomalies obtained in response to meltwater scenarios. The SSS adjustment overall reaches a new quasi-steady state in about 10 years, apart from that with the Greenland melt-rate of 5000 Gt yr^{-1}, as shown in the time series of SSS (Supplementary Fig. 2) and SSS anomaly (Figs. 1d-f). Due to the difference in land-ocean distribution and ocean circulation, surface freshening is confined to a small geographic area around Greenland, but extends over a larger area across the Southern Ocean. The freshwater pathways around Greenland simulated from our model show a plausible pattern in accord with Gillard et al. (2016). Specifically, freshwater release from west Greenland accumulates in Baffin Bay and then flows down the Labrador shelf; freshwater from east Greenland largely flows into the interior of the Labrador Sea, where deep convection occurs. Indeed, with Greenland meltwater, surface freshening spreads primarily along

TABLE 1. Experimental design for nine meltwater perturbation experiments.

Meltwater (MW) Forcing Schemes		500 Gt/yr (~0.016 Sv)	2000 Gt/yr (~0.06 Sv)	5000 Gt/yr (~0.16 Sv)
Scenarios (Ensemble Members)	Greenland MW	10	1	1
	Antarctic MW	10	1	1
	Greenland & Antarctic MW	10	1	1
Primary & Extended Periods		50 & 100 years	50 & 100 years	50 & 100 years
Distribution		Distributed evenly along the continental margins in the upper 200 m		

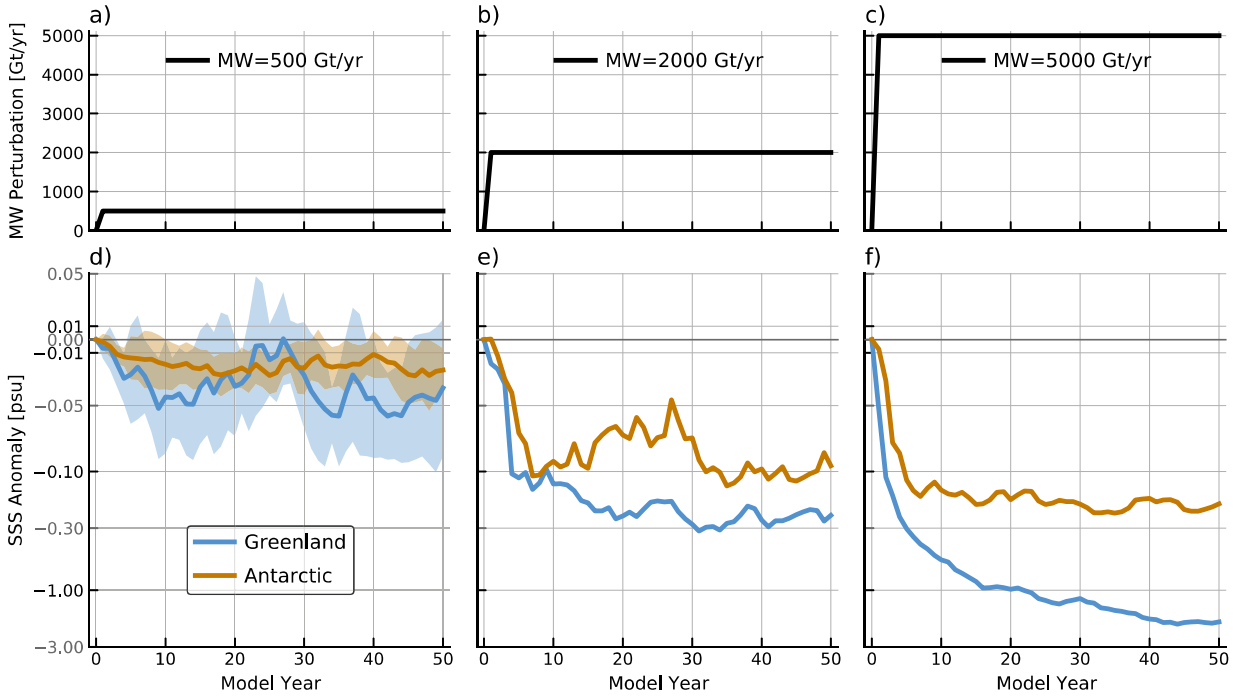

FIG. 1. Time series of step-change meltwater forcing perturbations of a) 500 Gt yr^{-1}, b) 2000 Gt yr^{-1} and c) 5000 Gt yr^{-1}, and d,e,f) corresponding SSS anomalies (psu) averaged over the North Atlantic sector (45°–80°N, 5°–65°W) in the Greenland scenario (blue) and the Southern Ocean sector (50°–90°S, 0°–360°E) in the Antarctic scenario (orange). Note that the y-axis scale of SSS anomalies in d,e,f) is non-linear. Shading in d) represents one standard deviation model spread for ten ensemble members, and the line represents the ensemble-mean in the 500 Gt yr^{-1} case. No standard deviation envelope is shown in e,f), due to only one ensemble member being employed.

the Labrador Current in the 500 Gt yr^{-1} and 2000 Gt yr^{-1} cases (Figs. 2a and 2c), but extends more widely across the subpolar North Atlantic in the 5000 Gt yr^{-1} case (Fig. 2e). As a result,

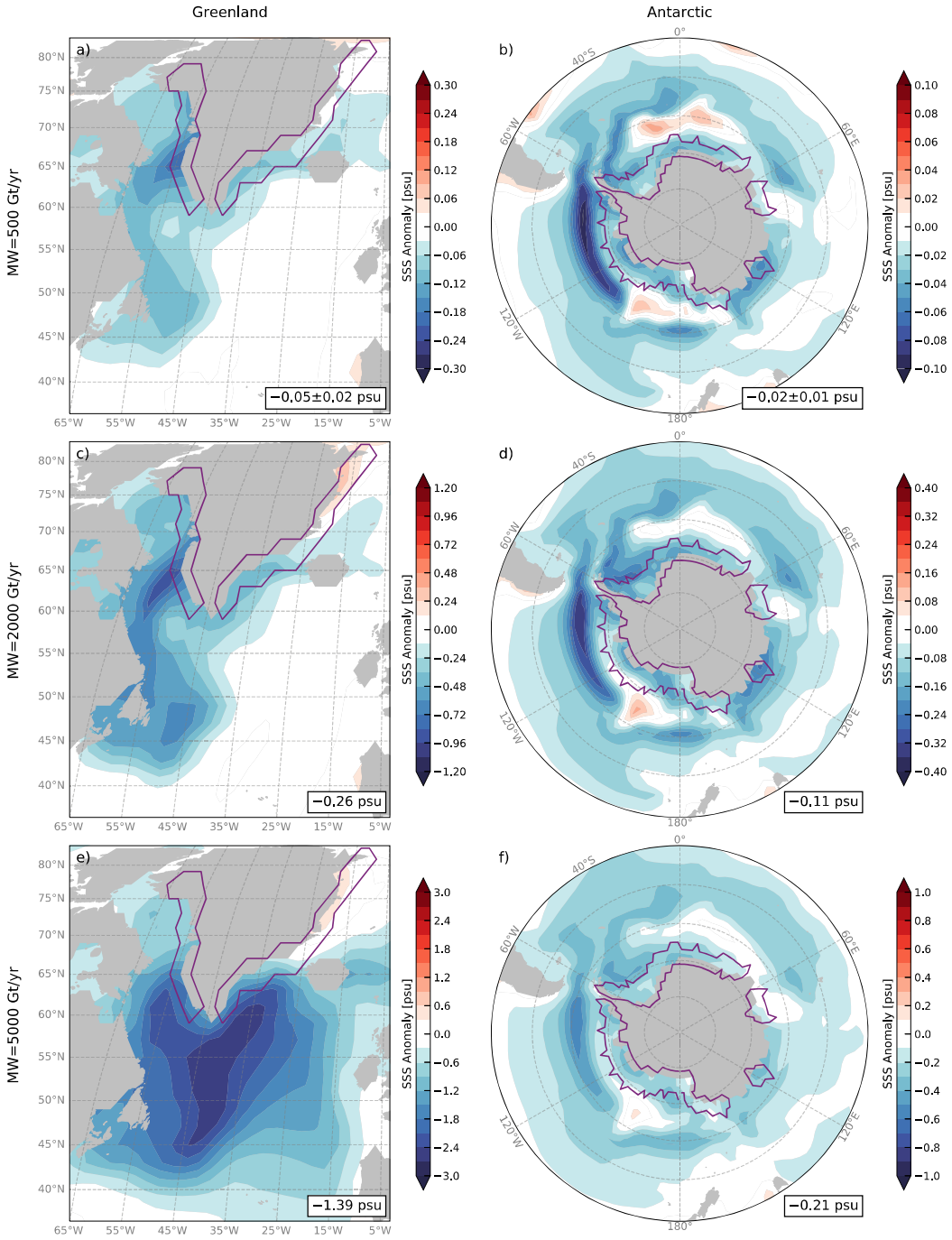

218 FIG. 2. SSS anomalies (psu) averaged over 50 years for a, c, e) the North Atlantic sector (45°–80°N, 5°–65°W)
219 in the Greenland scenario and b, d, f) the Southern Ocean sector (50°–90°S, 0°–360°E) in the Antarctic scenario
220 with meltwater forcings of 500 Gt yr^{-1}, 2000 Gt yr^{-1} and 5000 Gt yr^{-1}, respectively. Purple contours indicate the
221 mask of the Greenland and Antarctic iceberg arrays, where meltwater is fluxed into the ocean. Spatially-averaged
222 SSS anomalies (with one standard deviation for ten ensemble members in the 500 Gt yr^{-1} case) are indicated in
223 the boxes in the bottom right of each panel.

SSS decreases by -0.05 psu and -0.26 psu over the North Atlantic sector (45°–80°N, 5°–65°W) respectively in the 500 Gt yr^{-1} and 2000 Gt yr^{-1} cases, close to linear scaling. However, SSS dramatically decreases by -1.39 psu in the 5000 Gt yr^{-1} case. In contrast, with Antarctic meltwater spreading across the Southern Ocean, SSS anomaly is diluted and scales roughly linearly with the magnitude of three meltwater forcings: we observe the decreases of -0.02 psu, -0.11 psu and -0.21 psu over the Southern Ocean sector (50°–90°S, 0°–360°E), respectively (Figs. 2b, 2d and 2f). The linearity of the response, or otherwise, will be discussed in more detail in subsequent sections.

In the ocean interior, freshwater pathways are distinct between the Greenland and Antarctic scenarios. With Greenland meltwater, anomalous freshening largely penetrates to the deep ocean in the northern high-latitudes, although the Mediterranean Intermediate Water becomes saltier (Figs. 3a, 3c and 3e). With Antarctic meltwater, anomalous freshening extends down to 1-km depth in the southern mid-latitudes, following the pathways of formation and subduction of Subantarctic Mode Water and Antarctic Intermediate Water. However, the deep ocean becomes saltier around Antarctica (Figs. 3b, 3d and 3f).

3. Differing Global impacts of Greenland and Antarctic meltwater

a. Global surface response

To contrast the large-scale impacts of Greenland and Antarctic meltwater, surface air temperature anomalies from all nine perturbation experiments are presented in Fig. 4. Overall, surface air temperature experiences a substantial cooling, particularly local to the source of meltwater input. With the relatively small Greenland melt-rates of 500 Gt yr^{-1} and 2000 Gt yr^{-1}, anomalous surface cooling is apparent in the subpolar North Atlantic (Figs. 4a and 4b). As melt-rates increase to 5000 Gt yr^{-1}, anomalous surface cooling occurs across the entire Northern Hemisphere (Fig. 4c). As a result, the global-mean surface air temperature decreases by -0.01°C, -0.09°C and -0.68°C in the 500 Gt yr^{-1}, 2000 Gt yr^{-1} and 5000 Gt yr^{-1} cases, respectively (Figs. 4a-c). Note that the response is *greater* than what would be expected if the response was linear (super-linear) in the 5000 Gt yr^{-1} case (Fig. 4c). By comparison, with all three Antarctic melt-rates, anomalous surface cooling covers a wide area across the Southern Hemisphere. The global-mean surface air temperature decreases by -0.06°C, -0.25°C, and -0.46°C in the 500 Gt yr^{-1}, 2000 Gt yr^{-1} and 5000 Gt yr^{-1} cases, respectively (Figs. 4d-f). Note that the response, however, is *less* than what would

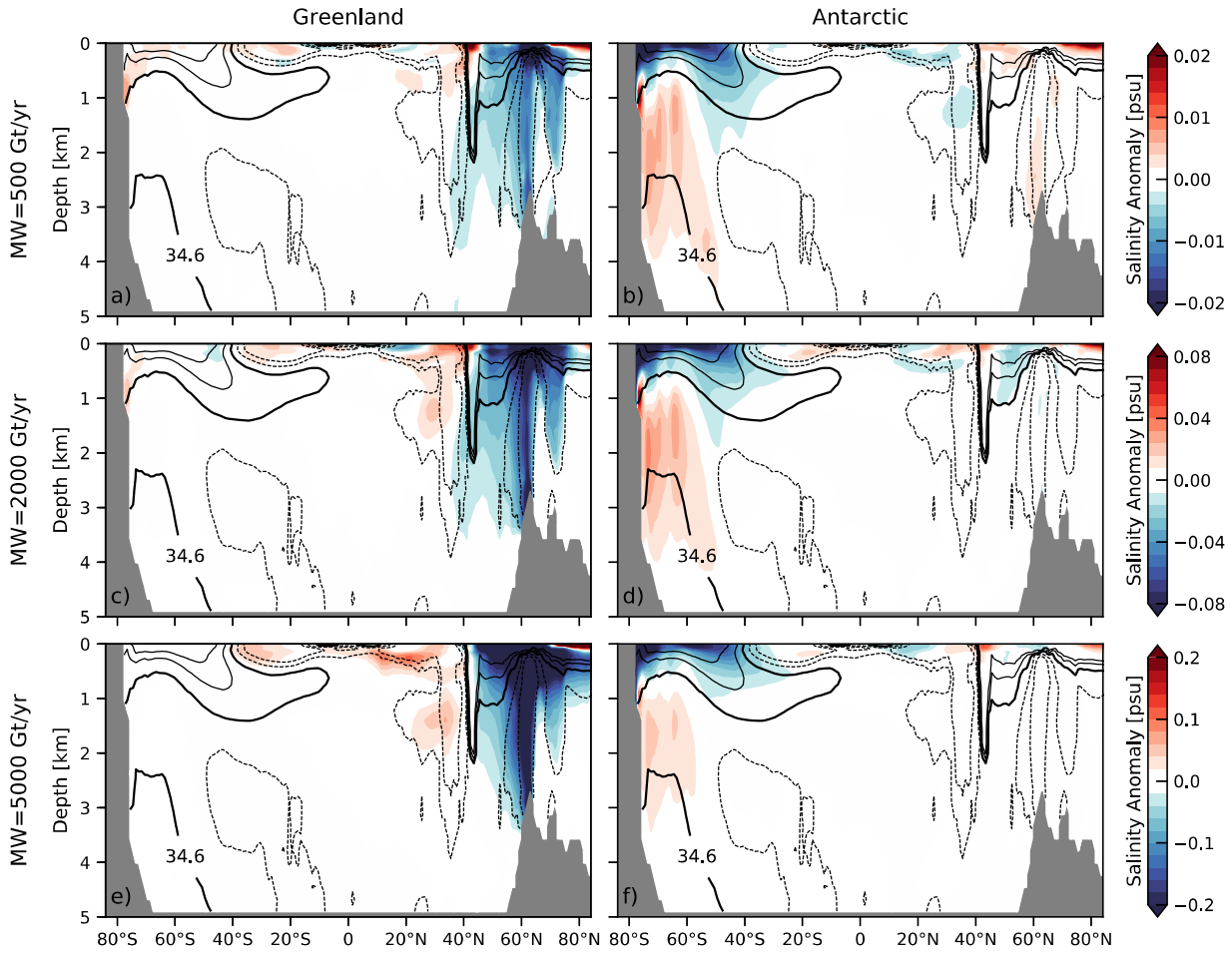

FIG. 3. Vertical cross-sections of the zonal-mean ocean salinity anomalies (psu; color) averaged over 50 years in the a, c, e) Greenland and b, d, f) Antarctic scenarios with meltwater forcings of 500 Gt yr^{-1}, 2000 Gt yr^{-1} and 5000 Gt yr^{-1}, respectively. Contours represent the climatological-mean ocean salinity from the control runs with an interval of 0.2 psu. The bold line is the 34.6 psu contour, marking the low-salinity tongue of Antarctic Intermediate Water extending to depth in the mid-latitudes of the Southern Ocean. Thin dashed and solid contours denote values above and below 34.6 psu (thick solid contour), respectively.

be expected if the response was linear (sub-linear) in the 5000 Gt yr^{-1} case (Fig. 4f). In sum, surface air temperature anomaly scales linearly with the forcing amplitude moving from 500 Gt yr^{-1} to 2000 Gt yr^{-1} but, as mentioned, this linear relationship breaks down in the 5000 Gt yr^{-1} case. Furthermore, surface air temperature anomaly in the simultaneous Greenland and Antarctic scenario is close to the sum of that in separate Greenland and Antarctic scenarios (Figs. 4g-i).

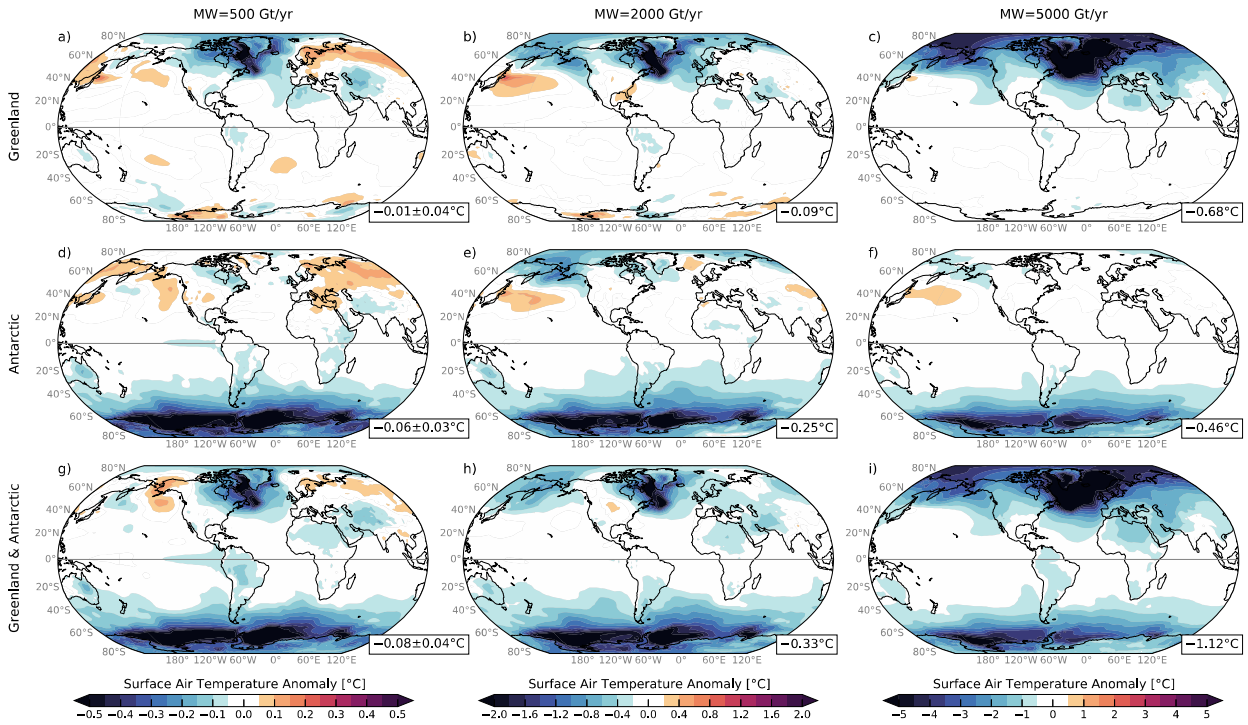

FIG. 4. Surface air temperature anomalies (°C) averaged over 50 years in the a, b, c) Greenland, d, e, f) Antarctic and g, h, i) simultaneous Greenland and Antarctic scenarios with meltwater forcings of 500 Gt yr^{-1}, 2000 Gt yr^{-1} and 5000 Gt yr^{-1}, respectively. Globally-averaged surface air temperature anomalies (with one standard deviation for ten ensemble members in the 500 Gt yr^{-1} case) are indicated in the boxes in the bottom right of each panel.

The global-scale cooling is dominated by Antarctic meltwater in the 500 Gt yr^{-1} and 2000 Gt yr^{-1} cases, but it is surpassed by Greenland meltwater in the 5000 Gt yr^{-1} case.

b. Atmospheric and ocean response

The zonal-mean atmospheric and ocean temperature anomalies are further examined (Fig. 5). In the atmosphere, meltwater drives anomalous cooling over the full vertical extent of the troposphere. With melt-rates of 500 Gt yr^{-1} and 2000 Gt yr^{-1}, the Antarctic-meltwater-driven cooling in the Southern Hemisphere is stronger and extends more equatorward to the tropics than the Greenland-meltwater-driven cooling in the Northern Hemisphere (Figs. 5a, 5b, 5d and 5e, top panels). As Greenland melt-rates increase to 5000 Gt yr^{-1}, atmospheric cooling intensifies dramatically and becomes super-linear in the Northern Hemisphere (Fig. 5c, top panel). Instead, as Antarctic

melt-rates increase to 5000 Gt yr^{-1}, atmospheric cooling in the Southern Hemisphere becomes sub-linear (Fig. 5f, top panel).

In the ocean, the temperature shows opposite responses to meltwater forcing in the two hemispheres: we observe the Greenland-meltwater-driven cooling north of 45°N and the Antarctic-meltwater-driven warming south of 45°S. As Greenland melt-rates increase from 500 Gt yr^{-1} through 2000 Gt yr^{-1} to 5000 Gt yr^{-1}, ocean cooling amplifies super-linearly (Figs. 5a-c, bottom panels). In contrast, ocean warming responds in a sub-linear way to three Antarctic melt-rates (Figs. 5d-f, bottom panels).

Meltwater also drives large-scale changes in atmospheric and ocean meridional overturning circulations (MOCs), shown in Fig. 6. Here we quantify the atmospheric MOC in sverdrups (Sv), where 1 Sv=10^9 kg s^{-1} (see e.g., Czaja and Marshall 2006). This definition is used because it enables us to use the same unit for both the atmosphere and ocean overturning streamfunctions. In addition, the ocean MOC is the total streamfunction that includes the eddy component. The climatological-mean atmospheric MOC contains three hemispherically symmetric cells: the Hadley cell, Ferrel cell and Polar cell. With meltwater from either Greenland or Antarctica, the atmospheric MOC anomaly shows a stronger Ferrel cell and a greater latitudinal extent for the equatorial Hadley Cell in each hemisphere (Figs. 6a-f, top panels). By comparison, these changes are more evident with the relatively large melt-rates.

Furthermore, the climatological-mean ocean MOC includes two global-scale thermohaline overturning cells: an upper cell linked to the AMOC and a lower cell driven by AABW formation and export (Marshall and Speer 2012). With enhanced stratification due to meltwater injection, the upper and lower cells both experience a significant slowdown. As Greenland melt-rates increase from 500 Gt yr^{-1} through 2000 Gt yr^{-1} to 5000 Gt yr^{-1}, the upper cell declines super-linearly (Figs. 6a-c, bottom panels). However, the lower cell is weakened in a sub-linear way to three Antarctic melt-rates (Figs. 6d-f, bottom panels).

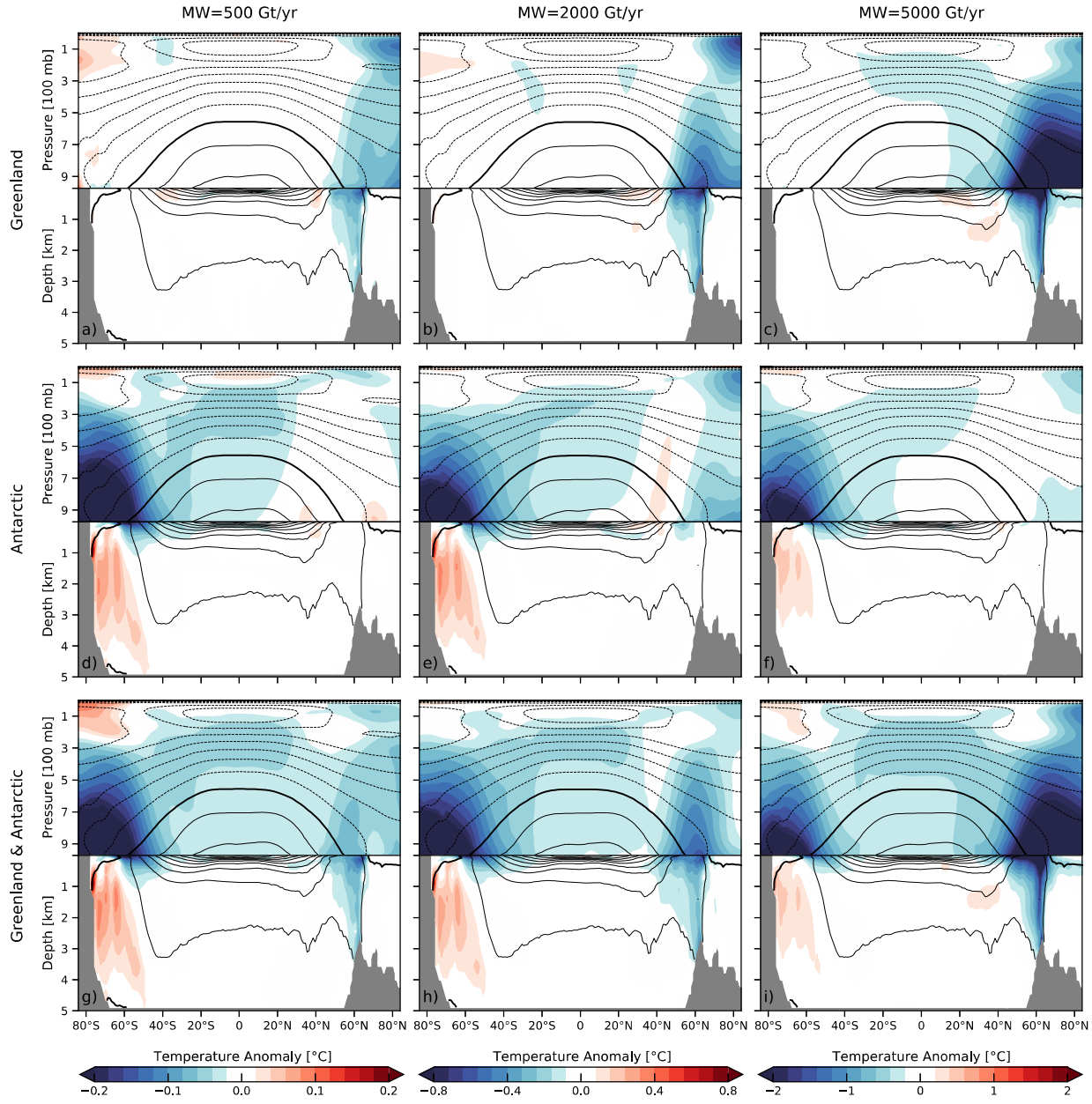

281 FIG. 5. Vertical cross-sections of the zonal-mean atmospheric and ocean temperature anomalies (°C; color)
282 averaged over 50 years in the a, b, c) Greenland, d, e, f) Antarctic and g, h, i) simultaneous Greenland and
283 Antarctic scenarios with meltwater forcings of 500 Gt yr^{-1}, 2000 Gt yr^{-1} and 5000 Gt yr^{-1}, respectively. Contours
284 represent the climatological-mean atmospheric and ocean temperature from the control runs with intervals of
285 10 °C and 3 °C, respectively. Dashed, solid and bold contours denote the negative, positive and zero values,
286 respectively.

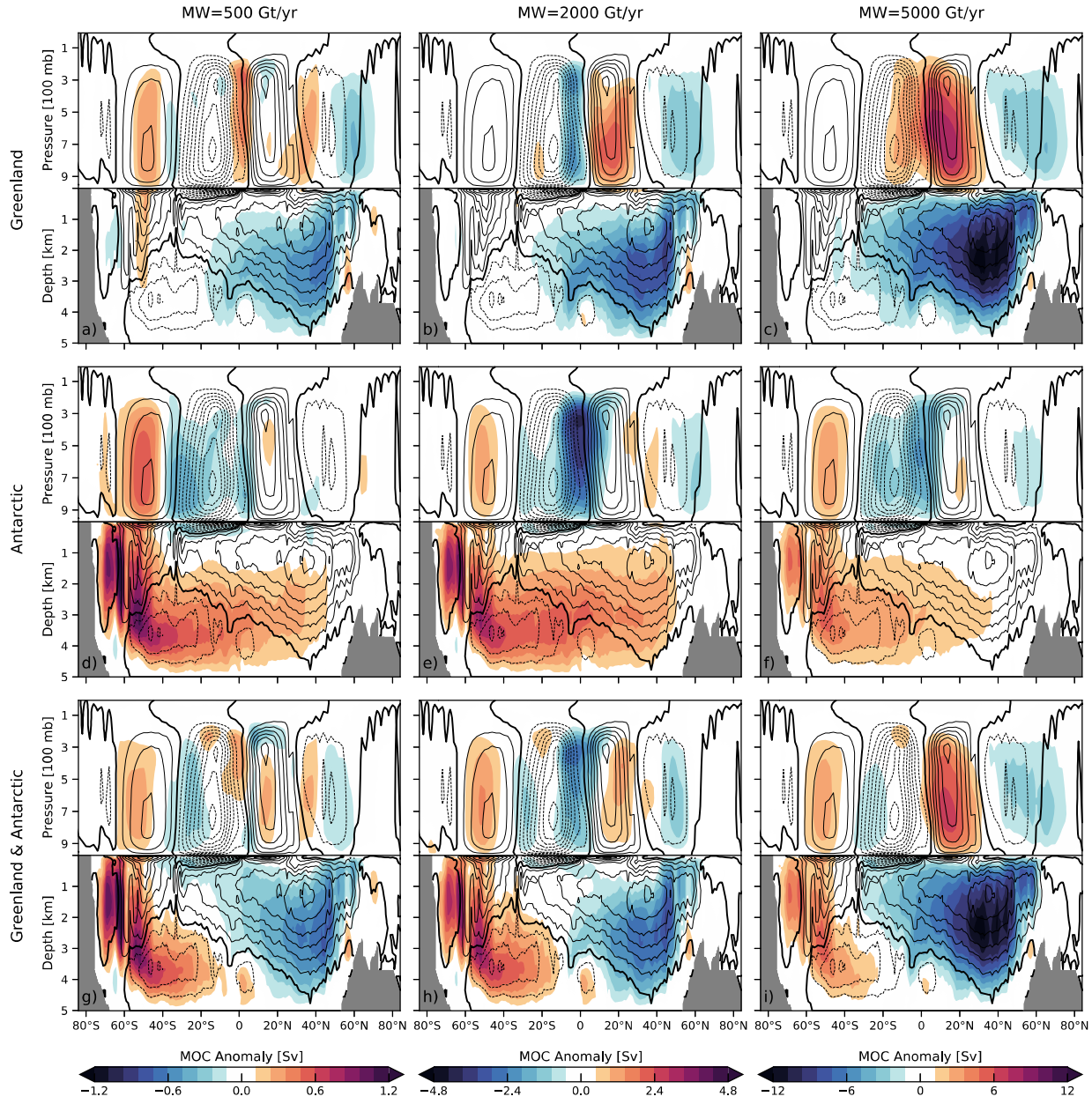

304 FIG. 6. Vertical cross-sections of the zonal-mean atmospheric and ocean MOC anomalies (Sv; color) averaged
305 over 50 years in the a, b, c) Greenland, d, e, f) Antarctic and g, h, i) simultaneous Greenland and Antarctic
306 scenarios with meltwater forcings of 500 Gt yr^{-1}, 2000 Gt yr^{-1} and 5000 Gt yr^{-1}, respectively. Contours represent
307 the climatological-mean atmospheric and ocean MOC from the control runs with intervals of 12 Sv and 4 Sv,
308 respectively. Dashed, solid and bold contours denote the negative (anticlockwise), positive (clockwise) and zero
309 values, respectively. The ocean MOC is represented as the total streamfuction that includes the eddy component.

4. Contrast of mechanisms controlling the climate response to Greenland and Antarctic meltwater

a. Sea ice response

The global impacts of Greenland and Antarctic meltwater are reflections of common but also distinct mechanisms at work in each hemisphere. First of all, an increase in sea-ice coverage is evident with meltwater from either Greenland or Antarctica (Fig. 7), associated with anomalous surface cooling (Fig. 4). With Greenland meltwater, anomalous surface cooling in the North Atlantic is likely due to diminished northward transport of heat caused by the AMOC slowdown (Buckley and Marshall 2016; Orihuela-Pinto et al. 2022). With Antarctic meltwater, instead, a lessening of vertical heat exchange due to enhanced upper-ocean stratification suppressing convection, causes anomalous surface cooling across the Southern Ocean (Richardson et al. 2005; Zhang 2007; Bintanja et al. 2013; Pauling et al. 2016). In addition, there are another two reasons for sea ice expansion: (i) an elevated freezing point of seawater due to enhanced surface freshening and cooling, and (ii) an increased percentage of incoming solar radiation reflected back to space via positive ice-albedo feedback.

With Antarctic meltwater, sea ice expands over a wide geographic area in longitude (Figs. 7b, 7d and 7f), coinciding with hemispheric surface cooling anomalies observed around Antarctica (Figs. 4d-f). In a recent study, Rye et al. (2022) highlighted that the widely distributed sea ice can reduce the water vapor transfer from the southern high-latitudes to the tropics, which can further drive a global-scale atmospheric cooling via negative water-vapor feedback. This Antarctic-meltwater-driven atmospheric cooling can compensate for greenhouse-gas-driven global warming by potentially 10 to 30% in the mid-century. In contrast, with Greenland meltwater, sea ice covers only a small area due to a different land-ocean distribution. For instance, sea ice grows mostly along the Labrador Sea in the 500 Gt yr^{-1} and 2000 Gt yr^{-1} cases (Figs. 7a and 7c), although it could also expand past over the Denmark Strait and across the Irminger Sea in the 5000 Gt yr^{-1} case (Fig. 7e). Note that within a 50-year time frame, sea-ice coverage is more geographically confined than that of hemispheric surface cooling (Figs. 4a-c). This indicates that other mechanisms for surface cooling in the Northern Hemisphere are likely at work in the Greenland scenario.

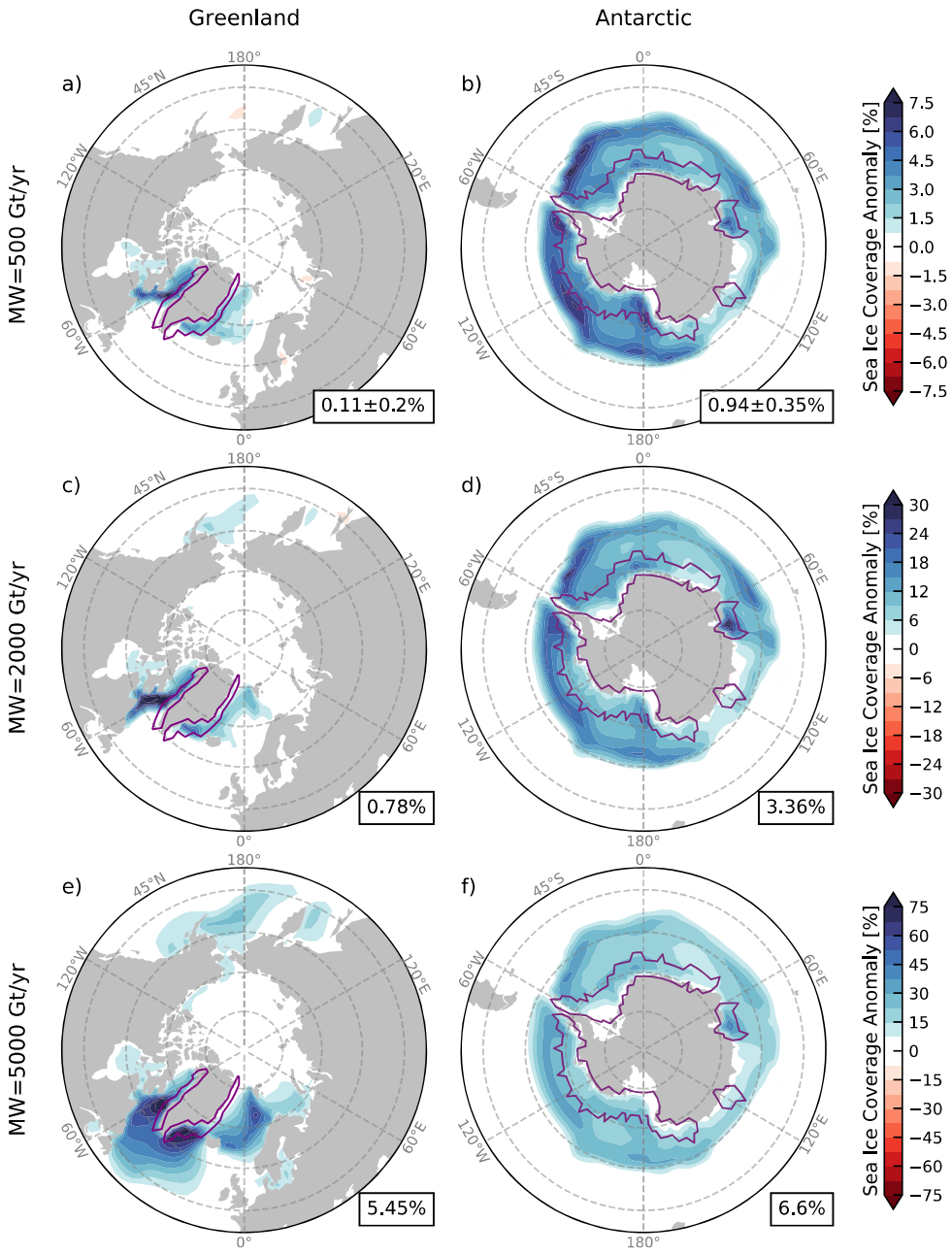

338 FIG. 7. Sea-ice coverage anomalies (%) averaged over 50 years for a, c, e) the Northern Hemisphere (NH)
339 in the Greenland scenario and b, d, f) the Southern Hemisphere (SH) in the Antarctic scenario with meltwater
340 forcings of 500 Gt yr^{-1}, 2000 Gt yr^{-1} and 5000 Gt yr^{-1}, respectively. Purple contours indicate the mask of the
341 Greenland and Antarctic iceberg arrays, where meltwater is fluxed into the ocean. Negative and positive values
342 indicate the sea-ice expansion and retreat, respectively. The NH (north of 45°N) and SH (south of 45°S) averages
343 of sea-ice coverage anomalies (with one standard deviation for ten ensemble members in the 500 Gt yr^{-1} case)
344 are indicated in the boxes in the bottom right of each panel.

The temporal evolution of sea-ice coverage is suggestive of different non-linear responses to Greenland and Antarctic meltwater. With Greenland meltwater, the sea-ice edge, referred to as the latitude of 15 percent sea-ice concentration, extends northward up to a latitude of 67°N in the 500 Gt yr^{-1} and 2000 Gt yr^{-1} cases (Figs. 8a and 8b), but extends dramatically beyond 53°N in the 5000 Gt yr^{-1} case (Figs. 8c and 8d). This sudden 'jump' suggests a super-linear response of sea-ice edge in the Northern Hemisphere to three Greenland melt-rates. With Antarctic meltwater, the sea-ice edge migrates northward gradually (Fig. 8h), but it cannot move too far north due to the presence of warm surface waters: it is found at 61°S, 59°S and 58.8°S in the 500 Gt yr^{-1}, 2000 Gt yr^{-1} and 5000 Gt yr^{-1} cases, respectively (Figs. 8e-g). This constrained Antarctic sea-ice edge, with a north limit of ~59°S, indicates a sub-linear response to three Antarctic melt-rates.

b. AMOC response

Another important mechanism is the influence of meltwater on the AMOC strength, which largely controls the magnitude of cross-equatorial heat transport and hence the asymmetric temperature response (Delworth et al. 1993; Stouffer et al. 2007; Marshall et al. 2014; Buckley and Marshall 2016). Here we define the AMOC strength as the maximum Atlantic overturning streamfunction at 45°N. Greenland meltwater contributes to a pronounced AMOC decline (Fig. 9a-c), which is in agreement with a recent observation-based inference (Rahmstorf et al. 2015) and many other modeling studies (Caesar et al. 2018; Thornalley et al. 2018; Boers 2021). The degree of AMOC decline is sensitive to Greenland melt-rates, and the response is non-linear. As Greenland melt-rates increase to 5000 Gt yr^{-1}, the AMOC strength decreases by a remarkable ~50% (-11.09 Sv) in 50 years (Fig. 9c). However, the AMOC strength is relatively insensitive to Antarctic melt-rates (Fig. 9d-f), increasing by only 0.32 Sv in the 5000 Gt yr^{-1} case (Fig. 9f)[1]. When both Greenland and Antarctic forcings are operative, the AMOC response is dominated by Greenland meltwater and shows a decline much as found when Greenland-only forcing is operative in 50 years (Figs. 9g-i)

We further show the temporal evolution of AMOC strength in Fig. 10. To examine the long-term variability of the AMOC, all the simulations are extended out to 150 years. With the two large meltwater forcings of 2000 Gt yr^{-1} and 5000 Gt yr^{-1}, the AMOC overall transits to another steady

[1]Weaver et al. (2003) argue that a change in the potential density relationship between the inflow of fresh Antarctic Intermediate Water (AAIW) and NADW can lead to enhanced formation of NADW and thence the AMOC.

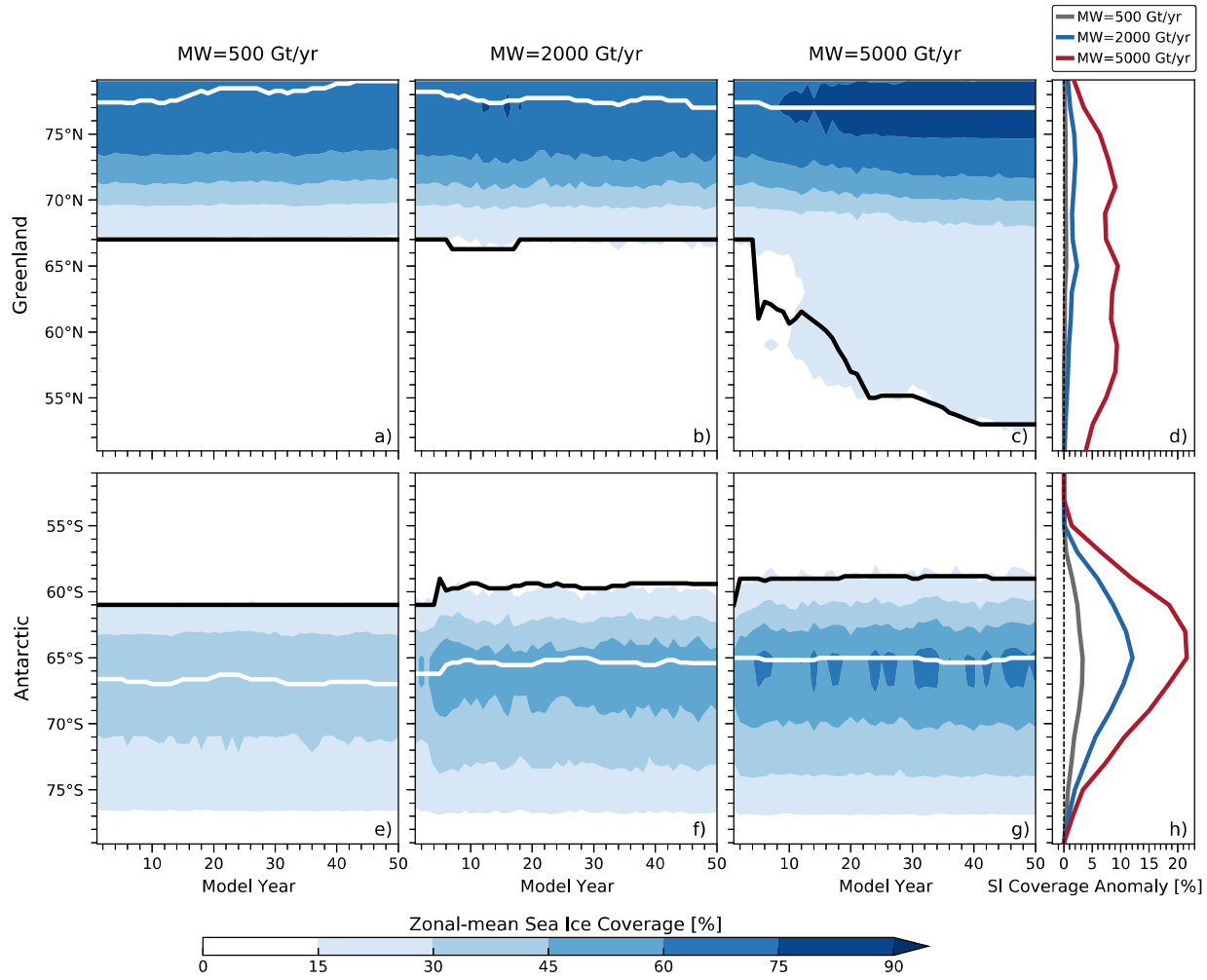

355 FIG. 8. Hovmöller diagram of the zonal-mean sea-ice coverage (%) over 50 years for a, b, c) the NH in the
356 Greenland scenario and e, f, g) the SH in the Antarctic scenario with meltwater forcings of 500 Gt yr^{-1}, 2000 Gt
357 yr^{-1} and 5000 Gt yr^{-1}, respectively. The zonal-mean sea-ice coverage anomalies (%) averaged over 50 years for
358 d) the NH in the Greenland scenario and h) the SH in the Antarctic scenario. Contours in a-c) and e-g) indicate
359 the latitude of maximum (marked in white) and 15 percent (black) sea-ice concentration after an 11-year moving
360 average.

385 state with some fluctuations but with reduced amplitude in about 50 years. With the Greenland
386 melt-rate of 2000 Gt yr^{-1}, the AMOC strength weakens by ~19.5% (-4.38 Sv) in 150 years, which
387 turns out to be not sufficient for a critical transition point to collapse (Fig. 10a). As Greenland
388 melt-rates increase to 5000 Gt yr^{-1}, the AMOC eventually collapses (Fig. 10a). In contrast, with
389 Antarctic meltwater, the AMOC anomaly exhibits more frequent fluctuations, and these fluctuations

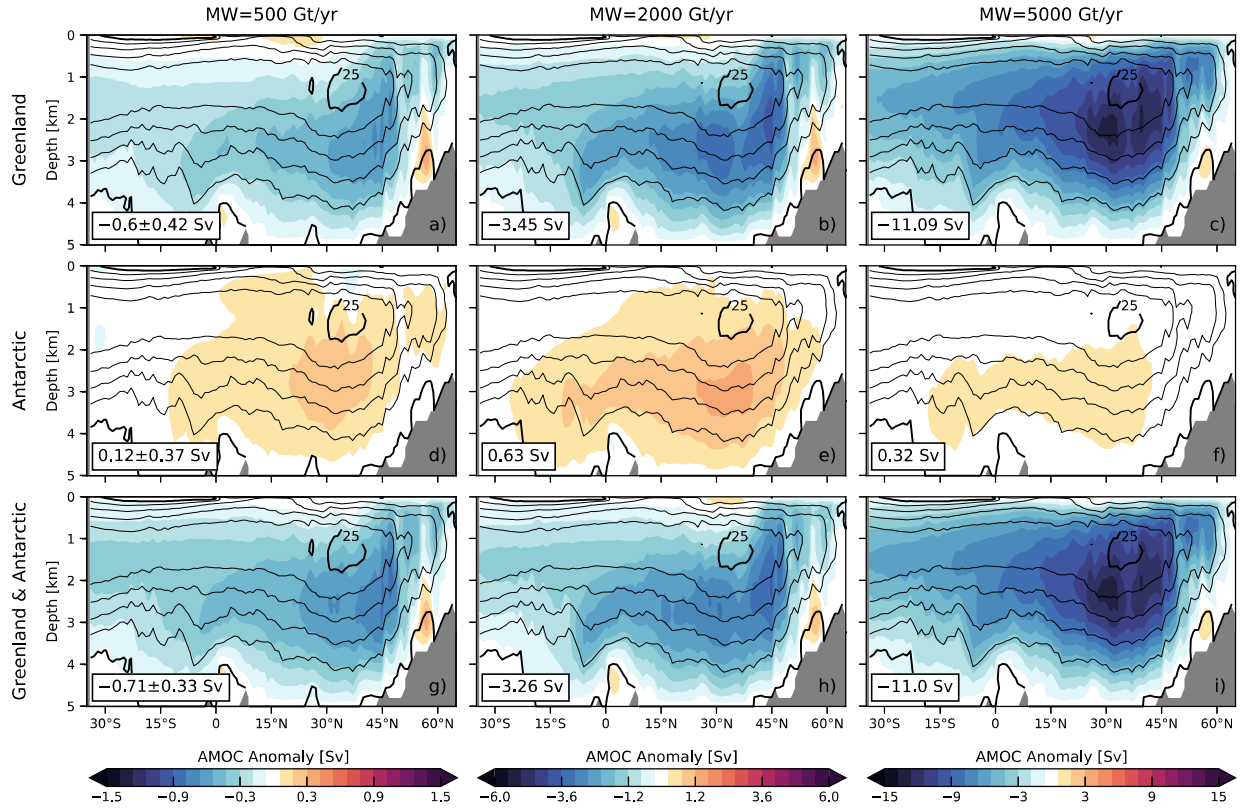

FIG. 9. Vertical cross-sections of the zonal-mean AMOC anomalies (Sv; color) averaged over 50 years in the a, b, c) Greenland, d, e, f) Antarctic and g, h, i) simultaneous Greenland and Antarctic scenarios with meltwater forcings of 500 Gt yr^{-1}, 2000 Gt yr^{-1} and 5000 Gt yr^{-1}, respectively. Contours represent the climatological-mean AMOC with an interval of 5 Sv and values of 0 Sv and 5 Sv in bold from the control runs. The AMOC strength anomalies (with one standard deviation for ten ensemble members in the 500 Gt yr^{-1} case) are indicated in the boxes in the bottom right of each panel.

dampen down over time (Fig. 10b). Again, the variability of AMOC strength is dominated by Greenland meltwater (Fig. 10c).

5. Response functions for meltwater forcing

a. Climate response functions

Figure 11 shows the time series and fitted CRF curves of anomalies in the surface air temperature, sea-ice extent, AMOC strength and AABW transport, all scaled per unit forcing. Here we define the AABW transport as the magnitude of the minimum global overturning streamfunction between

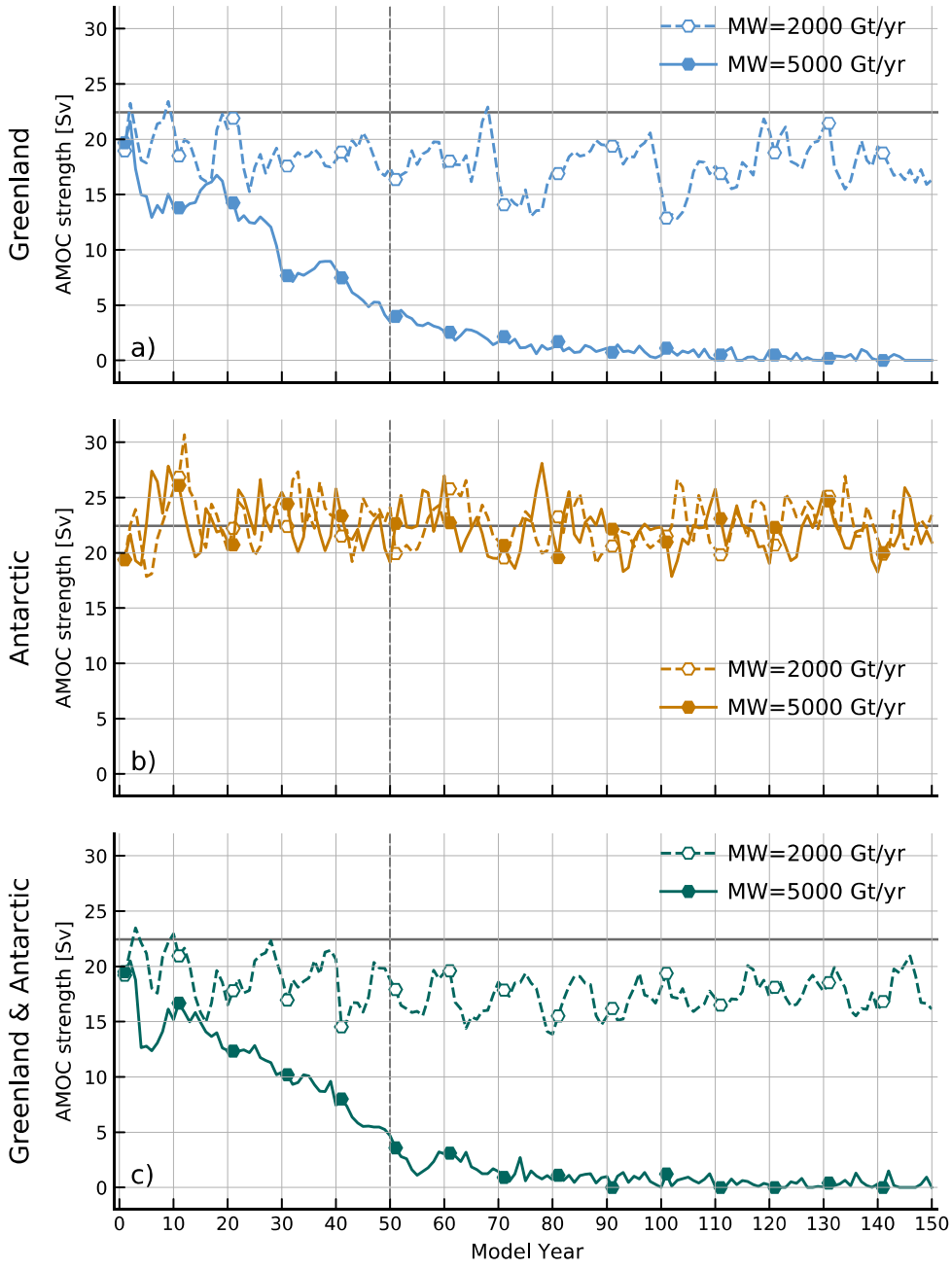

FIG. 10. Time series of the AMOC strength (Sv) in the a) Greenland (blue), b) Antarctic (orange) and c) simultaneous Greenland and Antarctic (green) scenarios with meltwater forcings of 2000 Gt yr^{-1} (dashed line with hollow circles) and 5000 Gt yr^{-1} (solid line with filled circles). Hollow and filled circles highlight the values every 10 years. The gray line denotes the climatological-mean AMOC strength of 22.45 Sv averaged over 150 years from the control run.

40°S and 50°S, which also reflects the strength of the lower cell. Plotted in this way, curves fall on top of one-another if the response scales linearly with the forcing amplitude moving from 500 Gt yr^{-1}, 2000 Gt yr^{-1} to 5000 Gt yr^{-1}. Analytical CRF curves are superimposed and constructed to fit the ensemble-means. Following Marshall et al. (2014), the fitted curves are calculated as the sum of two exponential functions corresponding to a 'fast' and 'slow' response, expressed as:

$$CRF \times F_{step} = T_f \left(1 - e^{-t/\tau_f}\right) + T_s \left(1 - e^{-t/\tau_s}\right), \quad (1)$$

where F_{step} (in Gt yr^{-1}) is the scaling factor representing the magnitude of the step-function in meltwater forcing, T_f and τ_f are the coefficients for the fast response, T_s and τ_s for the slow response, and t is the time in years.

From Fig. 11, we see that the CRFs of surface air temperature and sea-ice extent anomalies have a similar form in their respective hemispheres. For instance, with melt-rates of 500 Gt yr^{-1} and 2000 Gt yr^{-1}, the CRFs of surface cooling and sea-ice expansion show a linear response to Greenland meltwater in the Northern Hemisphere (Figs. 11a and 11g) and to Antarctic meltwater in the Southern Hemisphere (Figs. 11e and 11k). At these two forcing levels, the hemispheric response to Antarctic meltwater is greater than that to Greenland meltwater. However, with the Greenland melt-rate of 5000 Gt yr^{-1}, we observe massive surface cooling and sea-ice expansion in the Northern Hemisphere, leading to a super-linear response (Figs. 11a and 11g). This is a consequence of a dramatic decline and indeed collapse of the AMOC (Figs. 10a and 11m). In contrast, with the Antarctic melt-rate of 5000 Gt yr^{-1}, the response of surface cooling and sea-ice expansion in the Southern Hemisphere is sub-linear (Figs. 11e and 11k). This sub-linear response is likely due to the fact that the sea-ice edge cannot push further north of ~59°S (Figs. 8e-g), where surface waters out in the open ocean are too warm to sustain ice. Furthermore, Antarctic meltwater drives a significant reduction in AABW transport, analogous to the AMOC decline with Greenland meltwater. The CRFs of AABW transport anomalies also show a sub-linear response to Antarctic meltwater (Fig. 11q). Finally, by comparing with the CRFs in the simultaneous Greenland and Antarctic scenario, we see that Greenland and Antarctic meltwater plays the dominant role in their respective hemispheres (Fig. 11). The CRFs of all these climate parameters have no significant and persistent response in the other hemisphere, and thus are set to zero in the fitted curves (Figs. 11b, 11d, 11h, 11j, 11n and 11p).

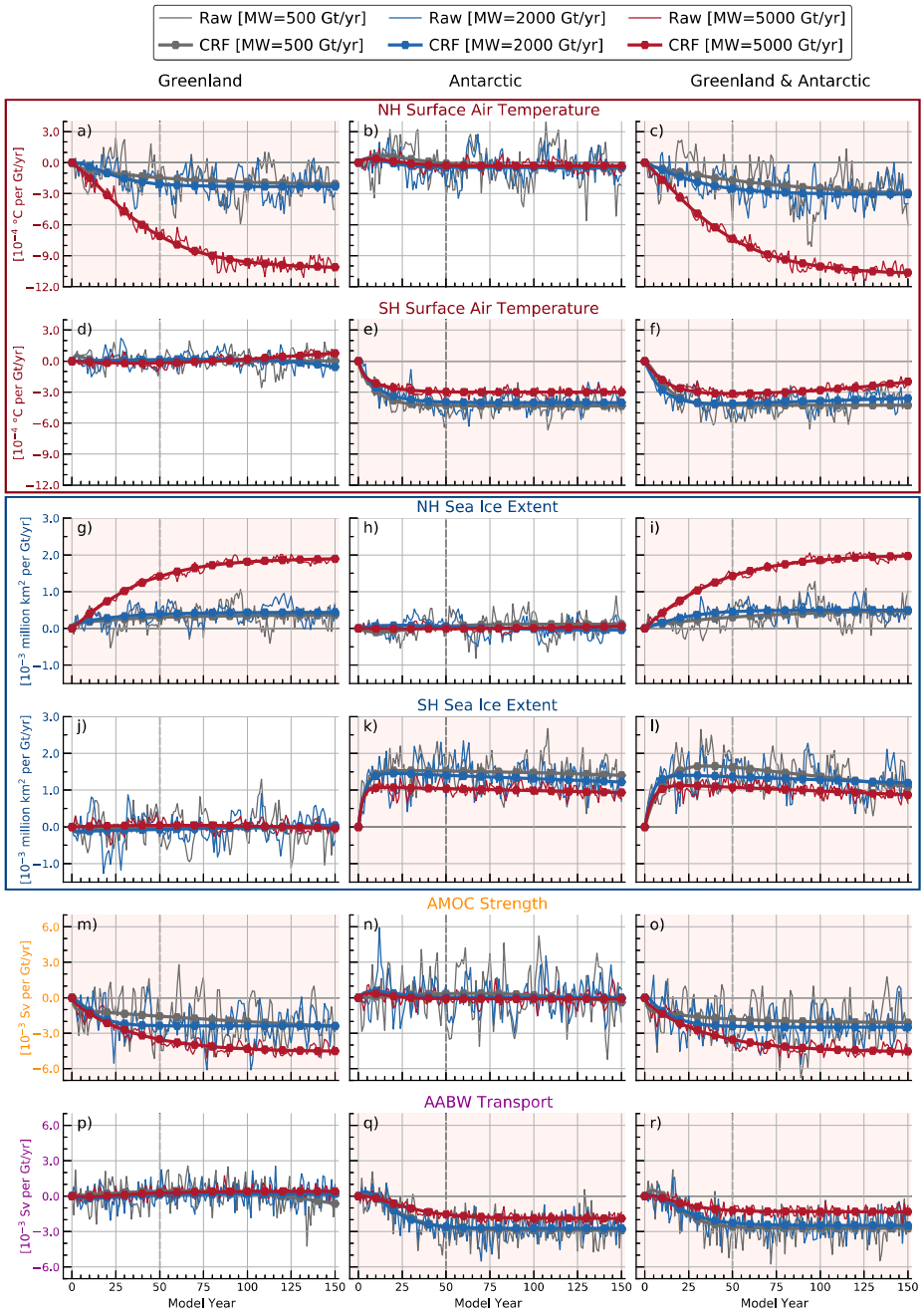

FIG. 11. Time series (thin line) and fitted curves, representing the CRFs (thick line with dots) of anomalies in the a, b, c) NH and d, e, f) SH surface air temperature (°C per Gt yr^{-1}), g, h, i) NH and j, k, l) SH sea-ice extent (million km^2 per Gt yr^{-1}), m, n, o) AMOC strength (Sv per Gt yr^{-1}) and p, q, r) AABW transport (Sv per Gt yr^{-1}). Note that all curves are scaled per unit forcing for meltwater forcings of 500 Gt yr^{-1} (gray), 2000 Gt yr^{-1} (blue) and 5000 Gt yr^{-1} (red), respectively. Analytical CRF curves are based on an exponential fit of raw time series. Light pink and white background shadings denote the significant (and persistent) and non-significant (close to a zero-line) CRFs, respectively. The NH and SH are defined as the region north of 23.5°N and south of 23.5°S, respectively, and thus exclude the tropics.

b. Projections based on linear convolution theory

By applying linear convolution theory, as set out in previous studies (Hasselmann et al. 1993; Marshall et al. 2014, 2017a), we can make projections of climate parameters of interest ($\mathcal{P}$) given a postulated time series of meltwater forcing perturbation, thus:

$$\mathcal{P}(t) = \int_0^t CRF|_{\mathcal{P}}(t-t') \frac{\partial F}{\partial t}(t')\, dt', \tag{2}$$

where F (in Gt yr^{-1}) is the prescribed time-series of meltwater forcing perturbation, $CRF|_{\mathcal{P}}$ (scaled per unit forcing) is the transient response of climate parameters to a step-change in meltwater forcing, and t is the time in years.

To make a projection, we first assume that the climate response depends linearly on meltwater forcing, which we have shown to be valid in scenarios with small to moderate meltwater forcings. We also assume that the ice mass loss results in net fluxes of meltwater to the proximal ocean. In addition, we must assume a forcing function $F(t)$ and its time-derivative ($\partial F/\partial t$) — required in Eq. (2) — for both Greenland and Antarctic scenarios. Ice mass loss-rates of both the Greenland and Antarctic ice sheets have been accelerating over recent decades: we estimate them using a linear regression based on satellite gravity observation since 2002 (Watkins et al. 2015). During the historical period 2002–2021, we find the loss-rates ($F|_{2002}$) to be 271 Gt yr^{-1} for Greenland and 145 Gt yr^{-1} for Antarctica (Fig. 12). Note that this Antarctic ice mass loss-rate is likely to be underestimated, because the satellite gravity observation cannot detect ice melting beneath ice shelves. Following the future projections based on the ice-sheet model simulations of Golledge et al. (2019), we assume the loss-rates in 2100 ($F|_{2100}$) to be 568 Gt yr^{-1} (0.018 Sv) for Greenland and 5047 Gt yr^{-1} (0.16 Sv) for Antarctica (Fig. 12). Using the loss-rates in 2002 ($F|_{2002}$) and 2100 ($F|_{2100}$), we obtain a gross estimate for a linear increase in forcing, yielding the constant time-derivatives ($\partial F/\partial t$) of 3 Gt yr^{-2} for Greenland and 50 Gt yr^{-2} for Antarctica. The $\partial F/\partial t$ is then used to carry out the integral in Eq. (2) after multiplying by the appropriate CRFs. Note that over the twenty-first century, Antarctic melt-rates range from 500 Gt yr^{-1} through 2000 Gt yr^{-1} to 5000 Gt yr^{-1}, reaching a level that is almost one order of magnitude greater than the Greenland melt-rate of 500 Gt yr^{-1}.

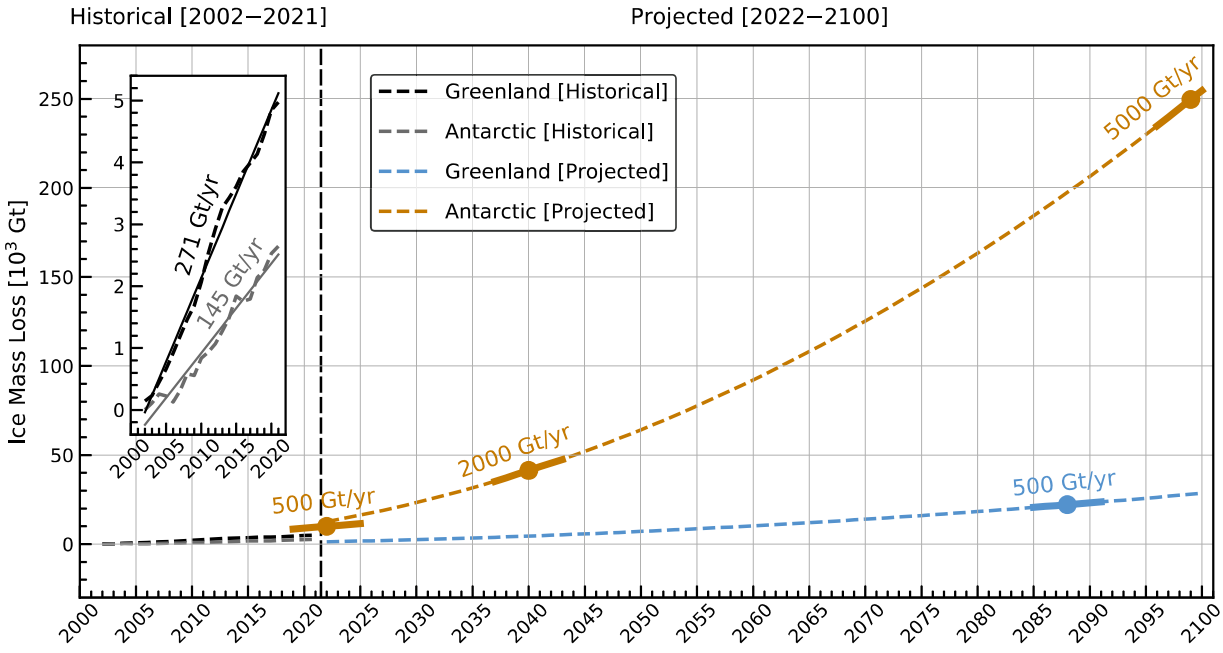

FIG. 12. Greenland (black and blue) and Antarctic (gray and orange) ice mass loss anomalies (Gt; dashed) relative to 2002 during the historical period 2002–2021 (Watkins et al. 2015) and projected forward from 2022–2100 under a high-emission scenario (Golledge et al. 2019). The inset box is a zoom on the historical period: the solid lines represent a linear regression of historical anomalies, yielding the constant loss-rates of 271 Gt yr^{-1} for Greenland (black) and 145 Gt yr^{-1} for Antarctica (gray). During the remainder of the twenty-first century, the projected loss-rates reach 500 Gt yr^{-1} around 2090 for Greenland (blue), and 500 Gt yr^{-1}, 2000 Gt yr^{-1} and 5000 Gt yr^{-1} around 2025, 2040 and 2100 for Antarctica (orange), respectively.

Figure 13 presents projections of climate parameters in response to Greenland and Antarctic meltwater, both separately and together, so that we can better contrast their relative contributions. We use the CRFs appropriate to the 500 Gt yr^{-1} curve for Greenland meltwater and 2000 Gt yr^{-1} curve for Antarctic meltwater. Consistent with our detailed calculations using the full model, Antarctic meltwater dominates in the Southern Hemisphere, inducing anomalous surface cooling, sea-ice expansion, and AABW contraction (Figs. 13b, 13d and 13f). Greenland meltwater dominates in the Northern Hemisphere, but anomalous surface cooling and sea-ice expansion are roughly one to two orders of magnitude smaller (Figs. 13a and 13c). Moreover, our projections suggest that by 2100, Greenland meltwater will cause only a small reduction of 0.45 Sv or so in the AMOC strength (Fig. 13e), but Antarctic meltwater will induce a great reduction of 10.2 Sv

in the AABW transport (Fig. 13f). Such a marked slowdown of the AABW formation could play a key role in abyssal ocean warming, as suggested in recent studies (Purkey and Johnson 2010; Li et al. 2023).

6. Conclusions and discussion

The Greenland and Antarctic ice sheets, including the floating ice shelves, have been melting and are likely to continue to melt at an accelerating rate over the twenty-first century (Fox-Kemper et al. 2021). Meltwater injection into the polar oceans is shown to have multiple significant large-scale climate impacts. These impacts express hemispheric asymmetries due to geographical differences that drive distinct feedback processes and response mechanisms. In this study, using a fully-coupled climate model, we have conducted nine step-function meltwater perturbation experiments, ranging from 500 Gt yr^{-1} through 2000 Gt yr^{-1} to 5000 Gt yr^{-1} for Greenland and Antarctica, both separately and together. This has enabled us to explore and contrast the global impacts of Greenland and Antarctic meltwater on the climate system.

A broad summary of the changes induced by meltwater discharge is shown in Fig. 14. In the atmosphere, meltwater from Greenland and Antarctica can both cause significant changes in temperature and circulation, such as cooling from the surface to the tropopause and strengthened Ferrel and Hadley cells (Fig. 14b, top panel). For melt-rates up to 2000 Gt yr^{-1}, the Antarctic-meltwater-driven changes are greater in magnitude and across a wider latitudinal extent. In the ocean, Greenland meltwater weakens the upper cell and NADW formation, associated with anomalous subsurface ocean cooling in the northern high-latitudes. Instead, Antarctic meltwater slows down the lower cell and AABW formation, associated with anomalous subsurface ocean warming around Antarctica (Fig. 14b, bottom panel). It should be noted that subsurface warming around Antarctica could further accelerate the basal melt of ice shelves (Pritchard et al. 2012; Rintoul et al. 2016), which has not been addressed in the present study.

Mechanisms controlling the climate response to Greenland and Antarctic meltwater are distinct. Antarctic meltwater drives surface cooling and sea-ice expansion across the Southern Hemisphere, by suppressing upper-ocean vertical heat exchange and positive ice-albedo feedback. A global-scale atmospheric cooling can further develop by reducing the water vapor transfer from the southern high-latitudes to the tropics (Rye et al. 2022). The climate response is rather linear for Antarctic

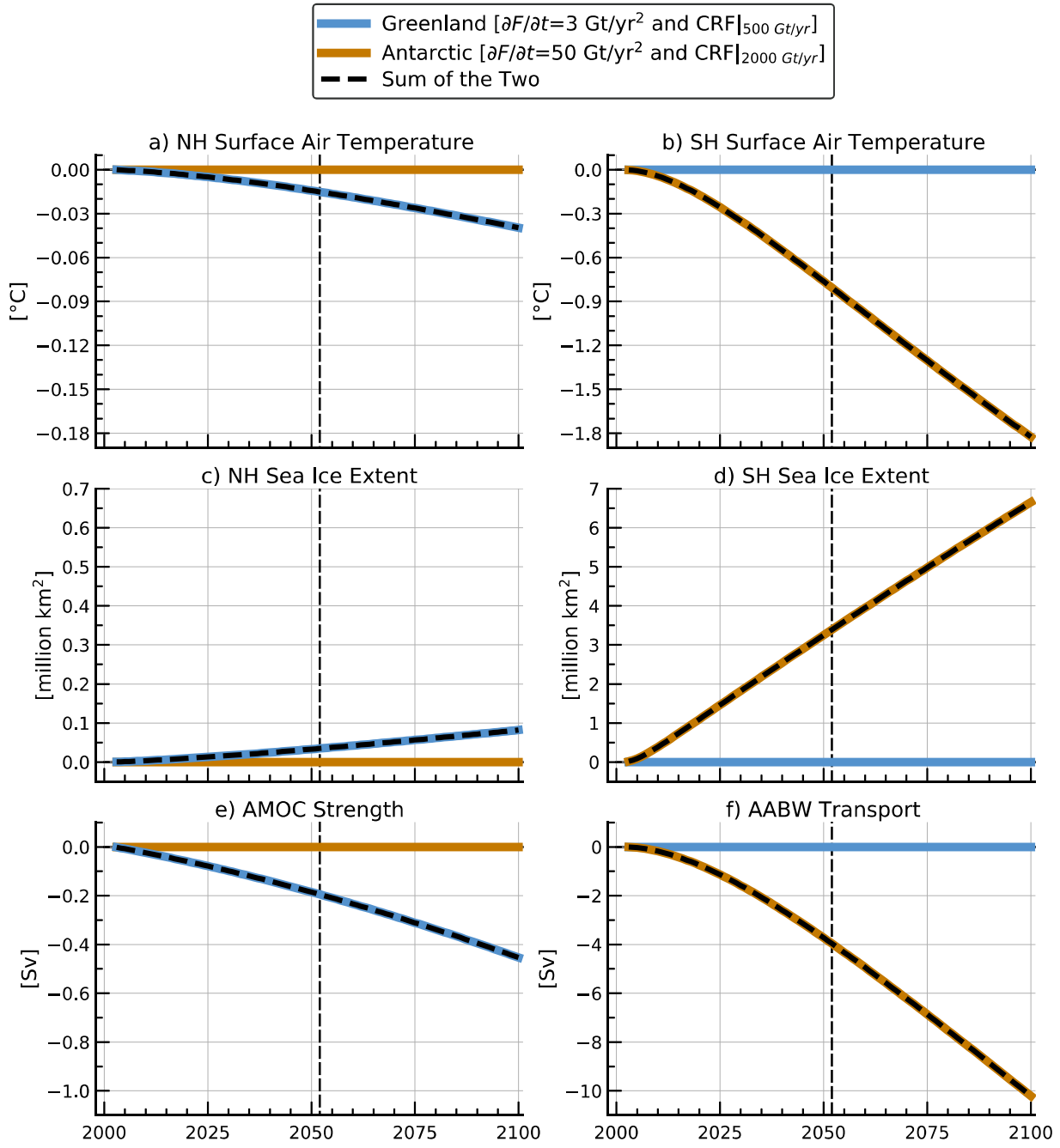

484 FIG. 13. Projections based on linear convolution for anomalies in the a) NH and b) SH surface air temperature
485 (°C), c) NH and d) SH sea-ice extent (million km^2), e) AMOC strength (Sv) and f) AABW transport (Sv).
486 The blue (orange) solid line represents the projection assuming $\partial F/\partial t$=3 Gt yr^{-2} (50 Gt yr^{-2}) using the CRF
487 appropriate to the 500 Gt yr^{-1} (2000 Gt yr^{-1}) curve for Greenland (Antarctic) meltwater. The black dashed line
488 represents the sum of two separate projections with Greenland (blue) and Antarctic (orange) meltwater.

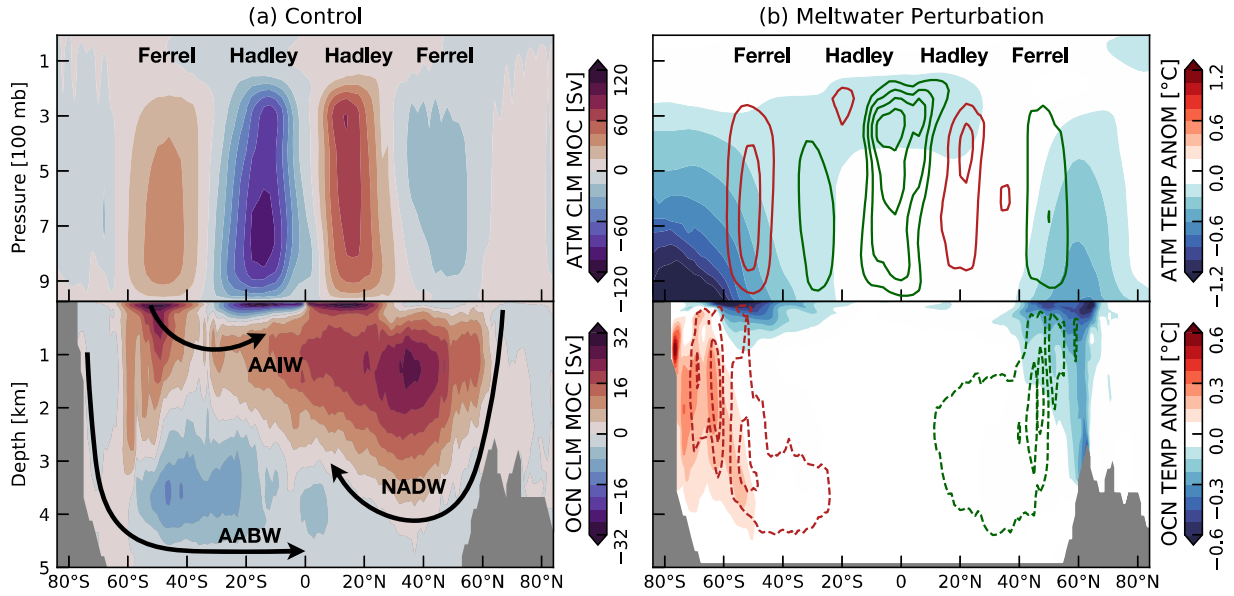

FIG. 14. Summary figure showing the climate response to Greenland and Antarctic meltwater: a) the climatological state of the atmosphere (top panel) and ocean (bottom panel), and b) changes in key quantities. Key circulation patterns are also labeled and indicated by arrows. Green contours indicate anticlockwise circulation; red contours clockwise circulation. Continuous contours indicate a strengthening of the preexisting circulation; dashed contours a weakening. Quantities plotted are vertical cross-sections of the zonal-mean a) climatological-mean MOC (Sv; color) of the atmosphere (top panel) and ocean (bottom panel) from the control run, and b) anomalies in temperature (°C; color) and MOC (Sv; color-coded contours) of the atmosphere (top panel) and ocean (bottom panel) averaged over 50 years from the simultaneous Greenland and Antarctic perturbation experiment with meltwater forcing of 2000 Gt yr^{-1}. Dark green and deep red solid contours in the top panel of b) respectively show the negative and positive values of atmospheric MOC anomalies from -2.4 Sv to 1.2 Sv with an interval of 0.6 Sv: these represent *strengthened* Hadley and Ferrel cells. Dark green and deep red dashed contours in the bottom panel of b) show the negative and positive values of ocean MOC anomalies from -3 Sv to 3 Sv with an interval of 1.5 Sv: these represent *weakened* upper and lower cells.

melt-rates up to 2000 Gt yr^{-1}, but ultimately becomes sub-linear with the larger melt-rate of 5000 Gt yr^{-1}. This is caused by the constrained sea-ice edge, as the continued expansion of sea ice outward is capped by the presence of warm waters to the north. In contrast, with Greenland meltwater, surface cooling and sea-ice expansion are more geographically confined in the Northern Hemisphere. There seem to be two reasons: First, sea-ice expansion is bounded to a smaller

geographic area in longitude; Second, surface cooling is also modulated by the AMOC slowdown, which reduces the poleward heat transport to the northern high-latitudes, with warming at lower latitudes that might counteract any reduced tropical cooling induced by water vapor. Moreover, the AMOC declines gradually for Greenland melt-rates up to 2000 Gt yr^{-1}, but eventually collapses with the larger melt-rate of 5000 Gt yr^{-1}. The AMOC collapse causes dramatic atmospheric and ocean changes: the climate response becomes amplifying and super-linear in the Northern Hemisphere. Note that the super-linear response of sea-ice expansion is also related to its own 'threshold' nature. As Greenland melt-rates increase to 5000 Gt yr^{-1}, sea ice moves sufficiently further south to a large area, where the sea surface temperatures are below the freezing point of seawater. Thus, once seawater freezes in that area allowing for greater effects on albedo and water vapor, surface cooling produces additional sea ice much more rapidly and super-linearly.

Finally, we contrast the relative contributions of Greenland and Antarctic meltwater through the analyses of CRFs and convolutions. Although Greenland dominates over Antarctic in the historical period (Shepherd et al. 2018, 2020), Antarctic melt-rate is projected to be at least one order of magnitude larger by 2100 (Golledge et al. 2019), due to its significant ice shelf-ocean interactions. Our results suggest that as the century proceeds, Antarctic meltwater will largely affect changes across the Southern Hemisphere, inducing anomalous surface cooling, sea-ice expansion, and the AABW contraction. By comparison, Greenland meltwater will still dominate the climate response across the Northern Hemisphere, but with a much smaller magnitude. In this assessment, the projected melt-rates are referenced to Golledge et al. (2019) under a high-emission scenario. This represents an upper bound on what might be possible. For this upper bound, the 'non-linearity' comes into effect early and, according to our analysis, the projected changes could be relatively large. Yet there remain many uncertainties in estimates of projected melt-rates. For instance, Golledge et al. (2019) presented ice-volume projections using initial conditions from coarse-resolution CMIP5 models. These models cannot accurately represent fine-scale processes, such as the waters that interact with the Antarctic shelf (Purich and England 2021). In addition, DeConto and Pollard (2016) also projected an ice-sheet retreat but with a much larger melt-rate of 15,800 Gt yr^{-1} (~0.5 Sv) for Antarctica in 2100 (see their Extended Data Fig. 8).

The goal of our study is to assess the climate impacts of meltwater discharge, and we therefore employ a fully-coupled climate model. While our model simulates distinct freshwater pathways

around Greenland and Antarctica, the ~1° horizontal resolution of our ocean model excludes mesoscale eddies and small-scale topographic features, which influence western boundary currents tight to the coast of the Labrador Sea (Gillard et al. 2022), shelf circulation and dense water formation around the Antarctic margins (Thompson et al. 2018; Morrison et al. 2020). In our model, most of the NADW formation is produced from the Labrador and Irminger Seas, much less from the GIN Seas than observed (Pickart and Spall 2007; Lozier et al. 2019), probably because the Iceland-Faroe Islands sills are too shallow to allow the dense water to spill into the North Atlantic. Our model simulates an AMOC that is somewhat stronger than observed (Miller et al. 2021), with a relatively rapid decline of the AMOC among CMIP6 models in response to global warming (Bellomo et al. 2021). In the context of this study, we detect some slight inter-hemispheric climate linkages driven by Antarctic meltwater, such as the abyssal warming extending across the equator after 50 years and ocean cooling in the north after 100 years (not shown). However, we do not find a clear response of the AMOC to Antarctic meltwater, which may be due to the limited duration of our experiments extending out to only 150 years. Despite the above caveats, our results robustly contrast the role of Greenland vs. Antarctic meltwater in instigating global climate change.

Acknowledgments. QL, JM, CR and AR are supported by the NASA MAP program 19-MAP19-0011 and the MIT-GISS cooperative agreement. The model simulations and analysis were conducted on the NASA High-End Computing (HEC) Program through the NASA Center for Climate Simulation (NCCS) at Goddard Space Flight Center.

Data availability statement. The data sets analyzed in this study will be all publicly available. Model components are all open source. The GISS modelE is available at `https://www.giss.nasa.gov/tools/modelE/`. The Greenland and Antarctic ice mass data from satellite observations were obtained for the period 2002–2021 at `https://climate.nasa.gov/vital-signs/ice-sheets/`.

References

Adusumilli, S., H. A. Fricker, B. Medley, L. Padman, and M. R. Siegfried, 2020: Interannual variations in meltwater input to the Southern Ocean from Antarctic ice shelves. *Nature Geoscience*, **13 (9)**, 616–620, https://doi.org/10.1038/s41561-020-0616-z.

Bakker, P., and M. Prange, 2018: Response of the intertropical convergence zone to Antarctic ice sheet melt. *Geophysical Research Letters*, **45 (16)**, 8673–8680, https://doi.org/https://doi.org/10.1029/2018GL078659.

Bakker, P., and Coauthors, 2016: Fate of the Atlantic Meridional Overturning Circulation: Strong decline under continued warming and Greenland melting. *Geophysical Research Letters*, **43 (23)**, 12,252–12,260, https://doi.org/https://doi.org/10.1002/2016GL070457.

Beadling, R. L., and Coauthors, 2022: Importance of the antarctic slope current in the southern ocean response to ice sheet melt and wind stress change. *Journal of Geophysical Research: Oceans*, **127 (5)**, e2021JC017 608, https://doi.org/https://doi.org/10.1029/2021JC017608.

Bellomo, K., M. Angeloni, S. Corti, and J. von Hardenberg, 2021: Future climate change shaped by inter-model differences in Atlantic meridional overturning circulation response. *Nature communications*, **12 (1)**, 3659–3659, https://doi.org/10.1038/s41467-021-24015-w.

Bintanja, R., G. J. van Oldenborgh, S. S. Drijfhout, B. Wouters, and C. A. Katsman, 2013: Important role for ocean warming and increased ice-shelf melt in Antarctic sea-ice expansion. *Nature Geoscience*, **6 (5)**, 376–379, https://doi.org/10.1038/ngeo1767.

Bitz, C. M., and W. H. Lipscomb, 1999: An energy-conserving thermodynamic model of sea ice. *Journal of Geophysical Research: Oceans*, **104 (C7)**, 15 669–15 677, https://doi.org/https://doi.org/10.1029/1999JC900100.

Boers, N., 2021: Observation-based early-warning signals for a collapse of the atlantic meridional overturning circulation. *Nature Climate Change*, **11 (8)**, 680–688, https://doi.org/10.1038/s41558-021-01097-4.

Böning, C. W., E. Behrens, A. Biastoch, K. J. Getzlaff, and J. L. Bamber, 2016: Emerging impact of Greenland meltwater on deepwater formation in the North Atlantic Ocean. *Nature Geoscience*, **9 (7)**, 523–527, https://doi.org/10.1038/ngeo2740.

Bronselaer, B., M. Winton, S. M. Griffies, W. J. Hurlin, K. B. Rodgers, O. V. Sergienko, R. J. Stouffer, and J. L. Russell, 2018: Change in future climate due to Antarctic meltwater. *Nature*, **564 (7734)**, 53–58, https://doi.org/10.1038/s41586-018-0712-z.

Buckley, M. W., and J. Marshall, 2016: Observations, inferences, and mechanisms of the Atlantic Meridional Overturning Circulation: A review. *Reviews of Geophysics*, **54 (1)**, 5–63, https://doi.org/https://doi.org/10.1002/2015RG000493.

Caesar, L., S. Rahmstorf, A. Robinson, G. Feulner, and V. Saba, 2018: Observed fingerprint of a weakening Atlantic Ocean overturning circulation. *Nature*, **556 (7700)**, 191–196, https://doi.org/10.1038/s41586-018-0006-5.

Czaja, A., and J. Marshall, 2006: The partitioning of poleward heat transport between the atmosphere and ocean. *Journal of the Atmospheric Sciences*, **63 (5)**, 1498–1511, https://doi.org/10.1175/JAS3695.1.

DeConto, R. M., and D. Pollard, 2016: Contribution of Antarctica to past and future sea-level rise. *Nature*, **531 (7596)**, 591–597, https://doi.org/10.1038/nature17145.

Delworth, T., S. Manabe, and R. J. Stouffer, 1993: Interdecadal variations of the thermohaline circulation in a coupled ocean-atmosphere model. *Journal of Climate*, **6 (11)**, 1993–2011, https://doi.org/10.1175/1520-0442(1993)006⟨1993:IVOTTC⟩2.0.CO;2.

Depoorter, M. A., J. L. Bamber, J. A. Griggs, J. T. M. Lenaerts, S. R. M. Ligtenberg, M. R. van den Broeke, and G. Moholdt, 2013: Calving fluxes and basal melt rates of Antarctic ice shelves. *Nature*, **502 (7469)**, 89–92, https://doi.org/10.1038/nature12567.

Eyring, V., S. Bony, G. A. Meehl, C. A. Senior, B. Stevens, R. J. Stouffer, and K. E. Taylor, 2016: Overview of the Coupled Model Intercomparison Project Phase 6 (CMIP6) experimental design and organization. *Geoscientific Model Development*, **9 (5)**, 1937–1958, https://doi.org/10.5194/gmd-9-1937-2016.

Fox-Kemper, B., and Coauthors, 2021: Ocean, cryosphere and sea level change. *Climate Change 2021: The Physical Science Basis. Contribution of Working Group I to the Sixth Assessment Report of the Intergovernmental Panel on Climate Change*, V. Masson-Delmotte, P. Zhai, A. Pirani, S. Connors, C. Péan, S. Berger, N. Caud, Y. Chen, L. Goldfarb, M. Gomis, M. Huang,

K. Leitzell, E. Lonnoy, J. Matthews, T. Maycock, T. Waterfield, O. Yelekçi, R. Yu, and B. Zhou, Eds., Cambridge University Press, Cambridge, United Kingdom and New York, NY, USA, chapter 9, 1211–1362, https://doi.org/10.1017/9781009157896.011.

Fretwell, P., and Coauthors, 2013: Bedmap2: improved ice bed, surface and thickness datasets for Antarctica. *The Cryosphere*, **7 (1)**, 375–393, https://doi.org/10.5194/tc-7-375-2013.

Gent, P. R., J. Willebrand, T. J. McDougall, and J. C. McWilliams, 1995: Parameterizing eddy-induced tracer transports in ocean circulation models. *Journal of Physical Oceanography*, **25 (4)**, 463–474, https://doi.org/10.1175/1520-0485(1995)025⟨0463:PEITTI⟩2.0.CO;2.

Gillard, L. C., X. Hu, P. G. Myers, and J. L. Bamber, 2016: Meltwater pathways from marine terminating glaciers of the Greenland ice sheet. *Geophysical Research Letters*, **43 (20)**, 10,873–10,882, https://doi.org/https://doi.org/10.1002/2016GL070969.

Gillard, L. C., C. Pennelly, H. L. Johnson, and P. G. Myers, 2022: The effects of atmospheric and lateral buoyancy fluxes on Labrador Sea mixed layer depth. *Ocean Modelling*, **171**, 101 974, https://doi.org/https://doi.org/10.1016/j.ocemod.2022.101974.

Golledge, N. R., E. D. Keller, N. Gomez, K. A. Naughten, J. Bernales, L. D. Trusel, and T. L. Edwards, 2019: Global environmental consequences of twenty-first-century ice-sheet melt. *Nature*, **566 (7742)**, 65–72, https://doi.org/10.1038/s41586-019-0889-9.

Gregory, J. M., T. Andrews, and P. Good, 2015: The inconstancy of the transient climate response parameter under increasing co¡sub¿2¡/sub¿. *Philosophical Transactions of the Royal Society A: Mathematical, Physical and Engineering Sciences*, **373 (2054)**, 20140 417, https://doi.org/10.1098/rsta.2014.0417.

Hasselmann, K., R. Sausen, E. Maier-Reimer, and R. Voss, 1993: On the cold start problem in transient simulations with coupled atmosphere-ocean models. *Climate Dynamics*, **9 (2)**, 53–61, https://doi.org/10.1007/BF00210008.

Hellmer, H. H., 2004: Impact of Antarctic ice shelf basal melting on sea ice and deep ocean properties. *Geophysical Research Letters*, **31 (10)**, https://doi.org/https://doi.org/10.1029/2004GL019506.

Hu, A., G. A. Meehl, W. Han, and J. Yin, 2011: Effect of the potential melting of the Greenland ice sheet on the meridional overturning circulation and global climate in the future. *Deep Sea Research Part II: Topical Studies in Oceanography*, **58 (17)**, 1914–1926, https://doi.org/https://doi.org/10.1016/j.dsr2.2010.10.069.

Jayne, S. R., 2009: The impact of abyssal mixing parameterizations in an ocean general circulation model. *Journal of Physical Oceanography*, **39 (7)**, 1756–1775, https://doi.org/10.1175/2009JPO4085.1.

Kelley, M., and Coauthors, 2020: GISS-E2.1: Configurations and climatology. *Journal of Advances in Modeling Earth Systems*, **12 (8)**, e2019MS002 025, https://doi.org/https://doi.org/10.1029/2019MS002025.

King, M. D., and Coauthors, 2020: Dynamic ice loss from the Greenland Ice Sheet driven by sustained glacier retreat. *Communications Earth & Environment*, **1 (1)**, 1, https://doi.org/10.1038/s43247-020-0001-2.

Lago, V., and M. H. England, 2019: Projected slowdown of Antarctic Bottom Water formation in response to amplified meltwater contributions. *Journal of Climate*, **32 (19)**, 6319–6335, https://doi.org/10.1175/JCLI-D-18-0622.1.

Large, W. G., J. C. McWilliams, and S. C. Doney, 1994: Oceanic vertical mixing: A review and a model with a nonlocal boundary layer parameterization. *Reviews of Geophysics*, **32 (4)**, 363–403, https://doi.org/https://doi.org/10.1029/94RG01872.

Lembo, V., V. Lucarini, and F. Ragone, 2020: Beyond forcing scenarios: Predicting climate change through response operators in a coupled general circulation model. *Scientific Reports*, **10 (1)**, 8668, https://doi.org/10.1038/s41598-020-65297-2.

Lerner, P., A. Romanou, M. Kelley, J. Romanski, R. Ruedy, and G. Russell, 2021: Drivers of air-sea CO_2 flux seasonality and its long-term changes in the NASA-GISS model CMIP6 submission. *Journal of Advances in Modeling Earth Systems*, **13 (2)**, e2019MS002 028, https://doi.org/https://doi.org/10.1029/2019MS002028.

Li, Q., M. H. England, A. M. Hogg, S. R. Rintoul, and A. K. Morrison, 2023: Abyssal ocean overturning slowdown and warming driven by Antarctic meltwater. *Nature*, **Accepted**.

Lozier, M. S., and Coauthors, 2019: A sea change in our view of overturning in the subpolar North Atlantic. *Science*, **363 (6426)**, 516–521, https://doi.org/10.1126/science.aau6592.

Mackie, S., I. J. Smith, J. K. Ridley, D. P. Stevens, and P. J. Langhorne, 2020: Climate response to increasing Antarctic iceberg and ice shelf melt. *Journal of Climate*, **33 (20)**, 8917–8938, https://doi.org/10.1175/JCLI-D-19-0881.1.

Marshall, J., K. C. Armour, J. R. Scott, Y. Kostov, U. Hausmann, D. Ferreira, T. G. Shepherd, and C. M. Bitz, 2014: The ocean's role in polar climate change: asymmetric Arctic and Antarctic responses to greenhouse gas and ozone forcing. *Philosophical Transactions of the Royal Society A: Mathematical, Physical and Engineering Sciences*, **372 (2019)**, 20130 040, https://doi.org/10.1098/rsta.2013.0040.

Marshall, J., J. Scott, and A. Proshutinsky, 2017a: "Climate response functions" for the Arctic ocean: a proposed coordinated modelling experiment. *Geoscientific Model Development*, **10 (7)**, 2833–2848, https://doi.org/10.5194/gmd-10-2833-2017.

Marshall, J., J. R. Scott, A. Romanou, M. Kelley, and A. Leboissetier, 2017b: The dependence of the ocean's MOC on mesoscale eddy diffusivities: A model study. *Ocean Modelling*, **111**, 1–8, https://doi.org/https://doi.org/10.1016/j.ocemod.2017.01.001.

Marshall, J., and K. Speer, 2012: Closure of the meridional overturning circulation through Southern Ocean upwelling. *Nature Geoscience*, **5 (3)**, 171–180, https://doi.org/10.1038/ngeo1391.

Miller, R. L., and Coauthors, 2021: CMIP6 historical simulations (1850–2014) with GISS-E2.1. *Journal of Advances in Modeling Earth Systems*, **13 (1)**, e2019MS002 034, https://doi.org/https://doi.org/10.1029/2019MS002034.

Morlighem, M., and Coauthors, 2017: Bedmachine v3: Complete bed topography and ocean bathymetry mapping of Greenland from multibeam echo sounding combined with mass conservation. *Geophysical Research Letters*, **44 (21)**, 11,051–11,061, https://doi.org/https://doi.org/10.1002/2017GL074954.

Morrison, A. K., A. M. Hogg, M. H. England, and P. Spence, 2020: Warm Circumpolar Deep Water transport toward Antarctica driven by local dense water export in canyons. *Science Advances*, **6 (18)**, eaav2516, https://doi.org/10.1126/sciadv.aav2516.

Mouginot, J., and Coauthors, 2019: Forty-six years of Greenland ice sheet mass balance from 1972 to 2018. *Proceedings of the National Academy of Sciences*, **116 (19)**, 9239–9244, https://doi.org/10.1073/pnas.1904242116.

Nazarenko, L. S., and Coauthors, 2022: Future climate change under ssp emission scenarios with giss-e2.1. *Journal of Advances in Modeling Earth Systems*, **In press**, e2021MS002 871, https://doi.org/https://doi.org/10.1029/2021MS002871.

Orihuela-Pinto, B., M. H. England, and A. S. Taschetto, 2022: Interbasin and interhemispheric impacts of a collapsed Atlantic Overturning Circulation. *Nature Climate Change*, **In press**, https://doi.org/10.1038/s41558-022-01380-y.

Paolo, F. S., H. A. Fricker, and L. Padman, 2015: Volume loss from Antarctic ice shelves is accelerating. *Science*, **348 (6232)**, 327–331, https://doi.org/10.1126/science.aaa0940.

Pauling, A. G., C. M. Bitz, I. J. Smith, and P. J. Langhorne, 2016: The response of the Southern Ocean and Antarctic sea ice to freshwater from ice shelves in an earth system model. *Journal of Climate*, **29 (5)**, 1655–1672, https://doi.org/10.1175/JCLI-D-15-0501.1.

Pickart, R. S., and M. A. Spall, 2007: Impact of Labrador Sea convection on the North Atlantic meridional overturning circulation. *Journal of Physical Oceanography*, **37 (9)**, 2207–2227, https://doi.org/10.1175/JPO3178.1.

Prather, M. J., 1986: Numerical advection by conservation of second-order moments. *Journal of Geophysical Research: Atmospheres*, **91 (D6)**, 6671–6681, https://doi.org/https://doi.org/10.1029/JD091iD06p06671.

Pritchard, H. D., S. R. M. Ligtenberg, H. A. Fricker, D. G. Vaughan, M. R. van den Broeke, and L. Padman, 2012: Antarctic ice-sheet loss driven by basal melting of ice shelves. *Nature*, **484 (7395)**, 502–505, https://doi.org/10.1038/nature10968.

Purich, A., and M. H. England, 2021: Historical and future projected warming of Antarctic Shelf Bottom Water in CMIP6 models. *Geophysical Research Letters*, **48 (10)**, e2021GL092 752, https://doi.org/https://doi.org/10.1029/2021GL092752.

Purkey, S. G., and G. C. Johnson, 2010: Warming of global abyssal and deep Southern Ocean waters between the 1990s and 2000s: Contributions to global heat and sea level rise budgets. *Journal of Climate*, **23 (23)**, 6336–6351, https://doi.org/10.1175/2010JCLI3682.1.

Putrasahan, D. A., K. Lohmann, J.-S. von Storch, J. H. Jungclaus, O. Gutjahr, and H. Haak, 2019: Surface flux drivers for the slowdown of the Atlantic Meridional Overturning Circulation in a high-resolution global coupled climate model. *Journal of Advances in Modeling Earth Systems*, **11 (5)**, 1349–1363, https://doi.org/https://doi.org/10.1029/2018MS001447.

Rahmstorf, S., J. E. Box, G. Feulner, M. E. Mann, A. Robinson, S. Rutherford, and E. J. Schaffernicht, 2015: Exceptional twentieth-century slowdown in Atlantic Ocean overturning circulation. *Nature Climate Change*, **5 (5)**, 475–480, https://doi.org/10.1038/nclimate2554.

Richardson, G., M. R. Wadley, K. J. Heywood, D. P. Stevens, and H. T. Banks, 2005: Short-term climate response to a freshwater pulse in the southern ocean. *Geophysical Research Letters*, **32 (3)**, https://doi.org/https://doi.org/10.1029/2004GL021586.

Rignot, E., S. Jacobs, J. Mouginot, and B. Scheuchl, 2013: Ice-shelf melting around Antarctica. *Science*, **341 (6143)**, 266–270, https://doi.org/10.1126/science.1235798.

Rignot, E., J. Mouginot, B. Scheuchl, M. van den Broeke, M. J. van Wessem, and M. Morlighem, 2019: Four decades of Antarctic ice sheet mass balance from 1979–2017. *Proceedings of the National Academy of Sciences*, **116 (4)**, 1095–1103, https://doi.org/10.1073/pnas.1812883116.

Rintoul, S. R., A. Silvano, B. Pena-Molino, E. van Wijk, M. Rosenberg, J. S. Greenbaum, and D. D. Blankenship, 2016: Ocean heat drives rapid basal melt of the Totten Ice Shelf. *Science Advances*, **2 (12)**, e1601 610, https://doi.org/10.1126/sciadv.1601610.

Russell, G. L., J. R. Miller, and D. Rind, 1995: A coupled atmosphere-ocean model for transient climate change studies. *Atmosphere-Ocean*, **33 (4)**, 683–730, https://doi.org/10.1080/07055900.1995.9649550.

Rye, C. D., J. Marshall, M. Kelley, G. Russell, L. S. Nazarenko, Y. Kostov, G. A. Schmidt, and J. Hansen, 2020: Antarctic glacial melt as a driver of recent Southern Ocean climate trends. *Geophysical Research Letters*, **47 (11)**, e2019GL086 892, https://doi.org/https://doi.org/10.1029/2019GL086892.

Rye, C. D., J. Marshall, D. Rind, G. A. Schmidt, and J. E. Hansen, 2022: Partial mitigation of global warming through Antarctic meltwater anomalies. *Science Advances*, **In revision**.

Schmidt, G. A., and Coauthors, 2014: Configuration and assessment of the giss modele2 contributions to the cmip5 archive. *Journal of Advances in Modeling Earth Systems*, **6 (1)**, 141–184, https://doi.org/https://doi.org/10.1002/2013MS000265.

Shepherd, A., and Coauthors, 2018: Mass balance of the Antarctic ice sheet from 1992 to 2017. *Nature*, **558 (7709)**, 219–222, https://doi.org/10.1038/s41586-018-0179-y.

Shepherd, A., and Coauthors, 2020: Mass balance of the Greenland ice sheet from 1992 to 2018. *Nature*, **579 (7798)**, 233–239, https://doi.org/10.1038/s41586-019-1855-2.

Silvano, A., S. R. Rintoul, B. Peña-Molino, W. R. Hobbs, E. van Wijk, S. Aoki, T. Tamura, and G. D. Williams, 2018: Freshening by glacial meltwater enhances melting of ice shelves and reduces formation of Antarctic Bottom Water. *Science Advances*, **4 (4)**, eaap9467, https://doi.org/10.1126/sciadv.aap9467.

Stouffer, R. J., D. Seidov, and B. J. Haupt, 2007: Climate response to external sources of freshwater: North Atlantic versus the Southern Ocean. *Journal of Climate*, **20 (3)**, 436–448, https://doi.org/10.1175/JCLI4015.1.

Thompson, A. F., A. L. Stewart, P. Spence, and K. J. Heywood, 2018: The Antarctic Slope Current in a changing climate. *Reviews of Geophysics*, **56 (4)**, 741–770, https://doi.org/https://doi.org/10.1029/2018RG000624.

Thornalley, D. J. R., and Coauthors, 2018: Anomalously weak Labrador Sea convection and Atlantic overturning during the past 150 years. *Nature*, **556 (7700)**, 227–230, https://doi.org/10.1038/s41586-018-0007-4.

Tournadre, J., N. Bouhier, F. Girard-Ardhuin, and F. Rémy, 2016: Antarctic icebergs distributions 1992–2014. *Journal of Geophysical Research: Oceans*, **121 (1)**, 327–349, https://doi.org/https://doi.org/10.1002/2015JC011178.

Visbeck, M., J. Marshall, T. Haine, and M. Spall, 1997: Specification of eddy transfer coefficients in coarse-resolution ocean circulation models. *Journal of Physical Oceanography*, **27 (3)**, 381–402, https://doi.org/10.1175/1520-0485(1997)027⟨0381:SOETCI⟩2.0.CO;2.

Watkins, M. M., D. N. Wiese, D.-N. Yuan, C. Boening, and F. W. Landerer, 2015: Improved methods for observing Earth's time variable mass distribution with GRACE using spherical cap mascons. *Journal of Geophysical Research: Solid Earth*, **120 (4)**, 2648–2671, https://doi.org/https://doi.org/10.1002/2014JB011547.

Weaver, A. J., O. A. Saenko, P. U. Clark, and J. X. Mitrovica, 2003: Meltwater pulse 1A from Antarctica as a trigger of the Bølling-Allerød warm interval. *Science*, **299 (5613)**, 1709–1713, https://doi.org/10.1126/science.1081002.

Zhang, J., 2007: Increasing Antarctic sea ice under warming atmospheric and oceanic conditions. *Journal of Climate*, **20 (11)**, 2515–2529, https://doi.org/10.1175/JCLI4136.1.

Zhang, J., and D. Rothrock, 2000: Modeling Arctic sea ice with an efficient plastic solution. *Journal of Geophysical Research: Oceans*, **105 (C2)**, 3325–3338, https://doi.org/https://doi.org/10.1029/1999JC900320.